Stem Cell Reports
Article
OPEN ACCESS

let-7 miRNAs Can Act through Notch to Regulate Human Gliogenesis

M. Patterson,[1,2,5] X. Gaeta,[1,2,3,5] K. Loo,[2] M. Edwards,[1] S. Smale,[1] J. Cinkornpumin,[1,2] Y. Xie,[1,2] J. Listgarten,[4] S. Azghadi,[2] S.M. Douglass,[1,2] M. Pellegrini,[1,2] and W.E. Lowry[1,2,3,*]

[1]Eli and Edythe Broad Center for Regenerative Medicine, UCLA, Box 957357, Los Angeles, CA 90095, USA
[2]Department of Molecular, Cell and Developmental Biology, UCLA, 621 Charles E. Young Drive East, Los Angeles, CA 90095, USA
[3]Molecular Biology Institute, UCLA, 611 Charles E. Young Drive East, Los Angeles, CA 90095, USA
[4]Microsoft Research, 1100 Glendon Avenue Suite PH1, Los Angeles, CA 90024, USA
[5]Co-first author
*Correspondence: blowry@ucla.edu
http://dx.doi.org/10.1016/j.stemcr.2014.08.015

SUMMARY

It is clear that neural differentiation from human pluripotent stem cells generates cells that are developmentally immature. Here, we show that the *let-7* plays a functional role in the developmental decision making of human neural progenitors, controlling whether these cells make neurons or glia. Through gain- and loss-of-function studies on both tissue and pluripotent derived cells, our data show that *let-7* specifically regulates decision making in this context by regulation of a key chromatin-associated protein, HMGA2. Furthermore, we provide evidence that the *let-7*/*HMGA2* circuit acts on *HES5*, a NOTCH effector and well-established node that regulates fate decisions in the nervous system. These data link the *let-7* circuit to NOTCH signaling and suggest that this interaction serves to regulate human developmental progression.

INTRODUCTION

We previously determined that, by both gene expression and functional analyses, the derivatives of human pluripotent stem cells (hPSCs) more closely resembled cell types found prior to 6 weeks of gestation than later time points (Patterson et al., 2012). In fact, this appears to be an emerging theme in hPSC differentiation (Chang et al., 2011; Mariani et al., 2012; Zambidis et al., 2005). This suggests that hPSC derivatives are developmentally immature, which could stem from either inadequate culturing methods or could suggest that developmental timing is somewhat conserved in vitro.

Among the most differentially expressed genes in all PSC derivatives are *LIN28A* and *LIN28B*, RNA binding proteins known to regulate the *let-7* family of miRNAs (Patterson et al., 2012). *LIN28B* seems to function primarily in the nucleus by sequestering *pri-let-7*s to prevent maturation by Microprocessor, whereas *LIN28A* functions in the cytoplasm by recruiting uridylyl transferase to polyuridylate the pre-*let-7*s and prevent their further processing by Dicer (Graf et al., 2013; Hagan et al., 2009; Kim and Nam, 2006; Lee et al., 2014; Piskounova et al., 2011). In lower organisms, *Lin28A* expression is strongly correlated with the differentiation status and self-renewing capacity of cells throughout development. Although there is less evidence for the role of this pathway in human development specifically, many groups have demonstrated that *LIN28A* is reexpressed in a variety of human cancers and is highly correlated with prognosis and disease progression (Viswanathan and Daley, 2010; West et al., 2009). Furthermore, *LIN28A* has also been used to reprogram somatic cells back to the pluripotent state (Yu et al., 2007). All of these known roles are linked to developmental progression and make *LIN28A/B-let-7* an attractive candidate for manipulating the maturity of hPSC-derived cells.

Previous work by other groups in lower organisms has argued that *Lin28A* plays a role in maturation of the nervous system (Balzer et al., 2010), and some have shown that overexpression of *LIN28B* in human adult hematopoietic stem/progenitor cells can reverse their developmental progression to a fetal-like state (Yuan et al., 2012). Downstream of LIN28A/B, however, a role for *let-7* in human gestational maturation in the nervous system has not been established. In fact, one study of a murine model has suggested that the role of *Lin28A* in developmental progression was *let-7* independent (Balzer et al., 2010). Recent work has also suggested that LIN28/*let-7* regulates neurogenesis by controlling the proliferation of progenitors (Cimadamore et al., 2013; Nishino et al., 2013). Here, we explore the role of the *LIN28*/*let-7* pathway in the developmental progression of human neural progenitor cells (NPCs). We demonstrate that *LIN28B* plays a clear role in gestational progression of the developing human nervous system through regulation of *let-7* miRNAs. These miRNAs then go on to regulate *HMGA2*, which has also been implicated in developmental progression (Sanosaka et al., 2008). We also show here that *HMGA2* appears to regulate cell-fate decisions in neural progenitors (NPCs) in this context

through *HES5*, a key node in the NOTCH pathway and previously implicated in neurogenesis.

RESULTS

PSC-NPCs Are Functionally and Transcriptionally Distinct from Tissue-Derived Counterparts

During mammalian development, NPCs progress through several phases: an early expansion phase, characterized by symmetric divisions; a neurogenic phase, characterized by asymmetric divisions and resulting in new neurons; a gliogenic phase where astrocytes are primarily produced; and finally a phase where oligodendrocytes are generated (Figure 1). The result is that neurogenesis precedes gliogenesis on a developmental timescale.

NPCs were derived from either hPSCs or from fetal tissue sources and were validated by immunostaining and judged to be relatively homogenous (Figure S1A; Patterson et al., 2012). We determined that PSC-NPCs across all passages had a higher propensity to differentiate into MAP2/TUJ1$^+$ neurons (~50%) over GFAP/S100/A2B5$^+$ glia (<10%) (Figure 1A). Meanwhile, tissue-derived NPCs isolated from fetal brain or spinal cord samples at 12–19 weeks of gestation (Tissue-NPCs) were more apt to differentiate into glia (~70%) over neurons (<20%) (Figure 1A; Patterson et al., 2012). These data suggest that PSC-NPCs were functionally less mature than tissue-derived counterparts (neurogenesis precedes gliogenesis). Furthermore, we have previously shown that upon subsequent passage of PSC-NPCs the propensity for gliogenesis increased but still did not approach that of tissue-derived cells (Patterson et al., 2012).

To understand the molecular basis for this observed functional discrepancy, gene expression profiling was performed on PSC derivatives and tissue-derived counterparts (Patterson et al., 2012). Among the most differentially expressed genes were *LIN28A* and *LIN28B* (Figures 1B, top, and S1C), and this was confirmed at the protein level by immunostaining (Figure 1B, bottom). Although continued passaging reduces the levels of *LIN28A* and *LIN28B* in PSC-NPCs, their expression is not decreased to a level found in the Tissue-NPCs within the time points utilized for this study (Figure 1B; Patterson et al., 2012).

LIN28 homologs are known to negatively regulate the highly conserved *let-7* family of miRNAs. Our previous microarray analyses demonstrated a significantly higher expression of some *let-7* miRNAs in Tissue-NPCs (Figure S1C), and this result was confirmed by direct sequencing of mature miRNA (Figure 1C; Table S1). The latter analysis demonstrated that not only were all *let-7* family members significantly higher in Tissue-NPCs, as we had previously shown by RT-PCR (Patterson et al., 2012), but all nine family members were found among the top 30 differentially expressed miRNAs between Tissue-NPCs and PSC-NPCs (Table S1). Furthermore, the *let-7* family as a whole was the most abundantly expressed miRNA family in 16 week Tissue-NPCs, representing almost 18% of the total miRNA in these cells. In addition, *let-7* family members were expressed at an intermediate level in 6–7 week Tissue-NPCs.

To determine whether *let-7* target genes were among the differentially expressed mRNA distinguishing PSC-NPCs from their tissue-derived counterparts, two lists of *let-7* targets were generated (Figure 1D): one with published *let-7* targets that have been experimentally confirmed (77 genes) and one with predicted *let-7* targets generated by TargetScan 5.2 (751 genes). Of the 77 published *let-7* targets, 20 were differentially expressed between PSC-NPCs and Tissue-NPCs, and 134 of the 751 TargetScan predicted *let-7* targets were differentially expressed. Notably, 95% and 63%, respectively, were specifically lower in Tissue-NPCs, consistent with a negative regulatory activity of *let-7* in tissue-NPCs.

Recent work in mice has suggested that during neurogenesis, the induction of *let-7* leads to exit of the cell cycle and differentiation toward neurons (Cimadamore et al., 2013; Nishino et al., 2013). Analysis of eight tissue-derived NPCs and three PSC-derived NPCs failed to find consistent differences in the percentage of cells in S or G2/M phase of the cell cycle (Figure 1E), suggesting that despite having orders of magnitude more *let-7* (Figure 1C), Tissue-NPCs can still maintain a proliferative state.

To determine when the transition from neurogenesis to gliogenesis occurs endogenously, we probed developmental transcriptome data for glial hallmark genes from the Allen Brain Atlas. GFAP, AQP4, and S100B were all expressed at a low level in all brain regions prior to 12 weeks but surged thereafter suggesting that gliogenesis begins in the human brain at roughly 12 weeks of gestation. A similar examination of oligodendrocyte markers suggests that oligodendrogenesis begins at 24 weeks (Figure 1F, middle). These gene expression data are consistent with pathological data on fetal tissue showing oligodendrocyte progenitors prevalent at 20 weeks of gestation and mature oligodendrocytes at 30 weeks (Craig et al., 2003; Dean et al., 2011; Jakovcevski et al., 2009). Notably, the expression of *LIN28B* in human brain was only detectable in weeks 8–9 of gestation and dropped off significantly thereafter (Figure 1F, middle), whereas *LIN28A* was undetectable in these analyses. *let-7* miRNAs were also detectable in these data sets, and this family showed a striking induction across the human brain in the 9–12 postconception week (PCW) time frame (Figure S1B). Taken together, these data suggested that there is a strong correlation between the transition from high*LIN28*/low*let-7* to low*LIN28*/high*let7* state

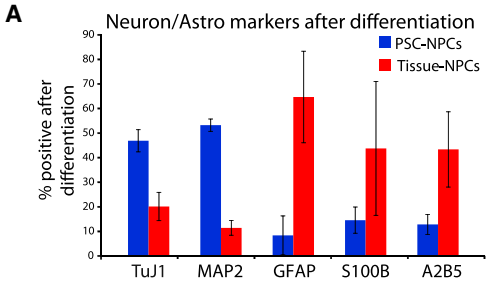

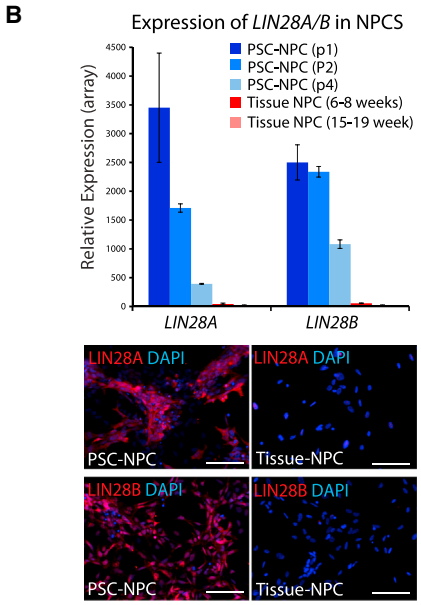

C

mature miRNA	16wk TissueNPC (average)	6-7wk TissueNPC (average)	PSC-NPC (average)	Fold Change (16wk Tissue v PSC-NPC)
let-7b	4.11%	1.00%	0.01%	460.76
let-7a	6.00%	1.89%	0.11%	52.55
let-7d	0.34%	0.33%	0.01%	43.53
let-7i	1.57%	0.80%	0.04%	43.51
miR-98	0.06%	0.03%	0.00%	24.65
let-7g	0.37%	0.12%	0.02%	23.60
let-7c	3.92%	3.98%	0.20%	19.24
let-7e	1.25%	1.35%	0.10%	12.40
let-7f	0.40%	0.10%	0.03%	12.33
Sum of all let-7 family	18.03%	9.61%	0.52%	34.67

D

	Total		let-7 published (77 genes)		TargetScan 5.2 let-7 (751 genes)	
	genes	% up in PSC-NPC	overlap	% up in PSC-NPC	overlap	% up in PSC-NPC
PSC-NPC vs Tissue-NPC	1885	44.4%	20	95.0%	134	62.7%

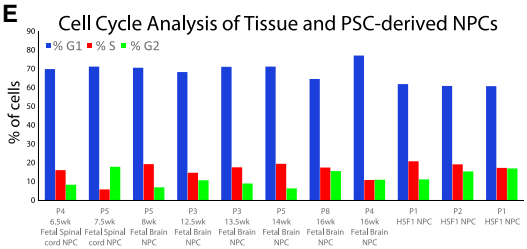

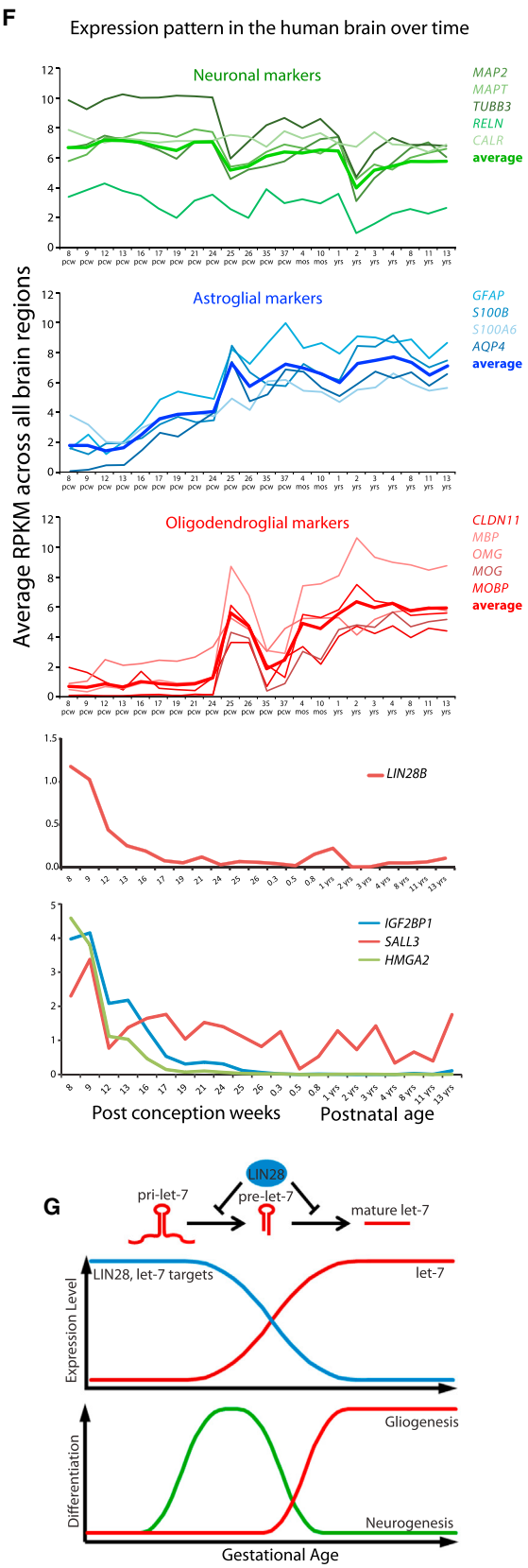

(legend on next page)

and the switch from neuro- to gliogenesis. Therefore, we hypothesized that the *let-7* plays a functional role in the decision to make either neurons or glia by neural progenitors (Figure 1G).

let-7 Expression and Processing across Development

LIN28A/B controls the maturation step to generate mature *let-7* (Hagan et al., 2009; Piskounova et al., 2008, 2011; Viswanathan et al., 2008), and *LIN28A* and *B* are also *let-7* targets. A priori, we expected that levels of *let-7* rose during development as a result of *LIN28A/B* downregulation over time. To understand the dynamics of *let-7* processing during development, we assessed the levels of pri, pre, and mature *let-7* miRNAs (Figure 2), we used RT-PCR to detect specifically mature *let-7* family members in NPCs and found that, similar to what was found by miRNA sequencing (miRNA-seq) profiling (Figure 1D), all *let-7* family members were dramatically higher in Tissue-NPCs compared to PSC-NPCs (Figure 2A; Patterson et al., 2012). Conversely, by using a miRNA RT-PCR approach that strictly measures primary *let-7* transcripts, we determined that *pri-let-7b* and *pri-let-7a2* transcript levels are significantly higher in Tissue-NPCs, whereas all the other tested members of the *let-7* family were essentially unchanged (Figure 2C). Similarly, a separate approach that can distinguish pri- and pre-*let-7* messages from mature *let-7* miRNAs also showed that pre-*let-7b* was the only *let-7* family member assayed that was differentially expressed in Tissue- versus PSC-NPCs (Figure 2B). Interestingly, *let-7b* and *let-7a3* are known to be expressed from the same locus (Wang et al., 2012), whereas *let-7a1* and *let-7a2* are transcribed from different loci.

Passaging of PSC-NPCs results in a decrease of both *LIN28A* and *LIN28B* (Figure 1B; Patterson et al., 2012) and increase of mature *let-7*s (Figure 2E; Patterson et al., 2012), suggesting a functional link between *LIN28* expression and levels of mature *let-7* as expected (Hagan et al., 2009; Heo et al., 2008). Interestingly, when assaying for pri-miRNA transcripts, many of the pri-*let-7*s were also induced during passaging as detected by both RT-PCR (Figure 2F) and Chromatin-RNA-seq (discussed more below; Figure 2G), which presumably occurred independently of any direct regulation by LIN28 protein, because they are not thought to play any role in regulation of transcription of pri-*let-7*s. These results point toward the existence of undescribed regulatory mechanisms governing *let-7* transcription independent of *LIN28* during human gestation.

To further verify the apparent transcriptional regulation of the *let-7* family, we employed an approach whereby chromatin-associated RNA is captured and sequenced (Bhatt et al., 2012). This approach generates data on relative amounts of nascent transcript, and therefore a bona fide measure of transcription as opposed to steady-state levels of RNA. Consistent with results from RT-PCR, transcription at the *let-7a3/let-7b* locus was significantly different between PSC-NPCs and Tissue-NPCs, demonstrating a *LIN28A/B* independent regulation of *let-7* (Figures 2D and 2G). These data also suggest that the *let-7* family of miRNAs is each subject to unique modes of transcriptional regulation that occurs prior to the actions of *LIN28A/B* on *let-7* maturation. Also shown is the expression of several unrelated miRNAs (miR-10, 15A, 15B) to demonstrate that the *let-7* effect is specific to this family and not indicative of imbalanced analysis (Figure 2G). This method allowed for a complete annotation of human *let-7* transcriptional loci based on analysis of transcribed RNA, as

Figure 1. *let-7* Activity Correlates with Human Gliogenesis

(A) Differentiation of human NPCs by growth factor withdrawal drives the generation of neurons and astrocytes. Percentage of positive PSC-NPCs and Tissue-NPCs (7–19 weeks of gestation) undergoing neuronal (TUJ1, MAP2) versus glial (GFAP, S100B, A2B5) differentiation. Error bars represent standard error of the mean (SEM) over three at least three biological replicates.

(B) Average expression of *LIN28A* and *LIN28B* probe sets from (Patterson et al., 2012). PSC-NPCs p1 (n = 7), PSC-NPCs p2 (n = 2), PSC-NPCs p4 (n = 2), 6–8 week tissue-NPCs (n = 6), 15–19 week fetal NPCs (n = 5). Error bars represent SEM over biological replicate lines. Scale bars, 100 μm.

(C) Percentage of contribution of *let-7* miRNA family members to all miRNA present in cells derived from 16 week Tissue-NPCs (n = 2), 6–7 week Tissue-NPCs (n = 2), and PSC-NPCs (n = 3) by miRNA-seq. Fold change of normalized expression between 16 week Tissue-NPCs and PSC-NPCs for each family member is shown at right. Data for all miRNAs can be found in Table S1.

(D) Genes differentially expressed between PSC-NPCs (n = 7) and Tissue-NPCs (n = 5) as identified (Patterson et al., 2012) and the number of *let-7* targets represented in the data. *let-7* target lists were generated from published articles and TargetScan 5.2.

(E) Despite having significantly different levels of *let-7*, PSC- and Tissue-NPCs show similar proliferative potential as measured by cell-cycle analysis based on propidium iodide staining and flow cytometry.

(F) RNA-seq data from the Allen Institute's Brainspan developmental transcriptome database displayed as log-scale reads per kilobase measured ($\log_2$ RPKM) across the developing human brain. Top, transcription of neuronal, glial and oligodendrocyte marker genes (the average of all markers indicated by boldface line); middle, transcription of *LIN28B*; bottom, transcription of selected *let-7* target genes.

(G) Top, schematic of *LIN28*'s role in the progression of *let-7* microRNAs and the pathway's temporal correlation with development. Bottom, differentiation propensity of NPCs correlated with gestational age.

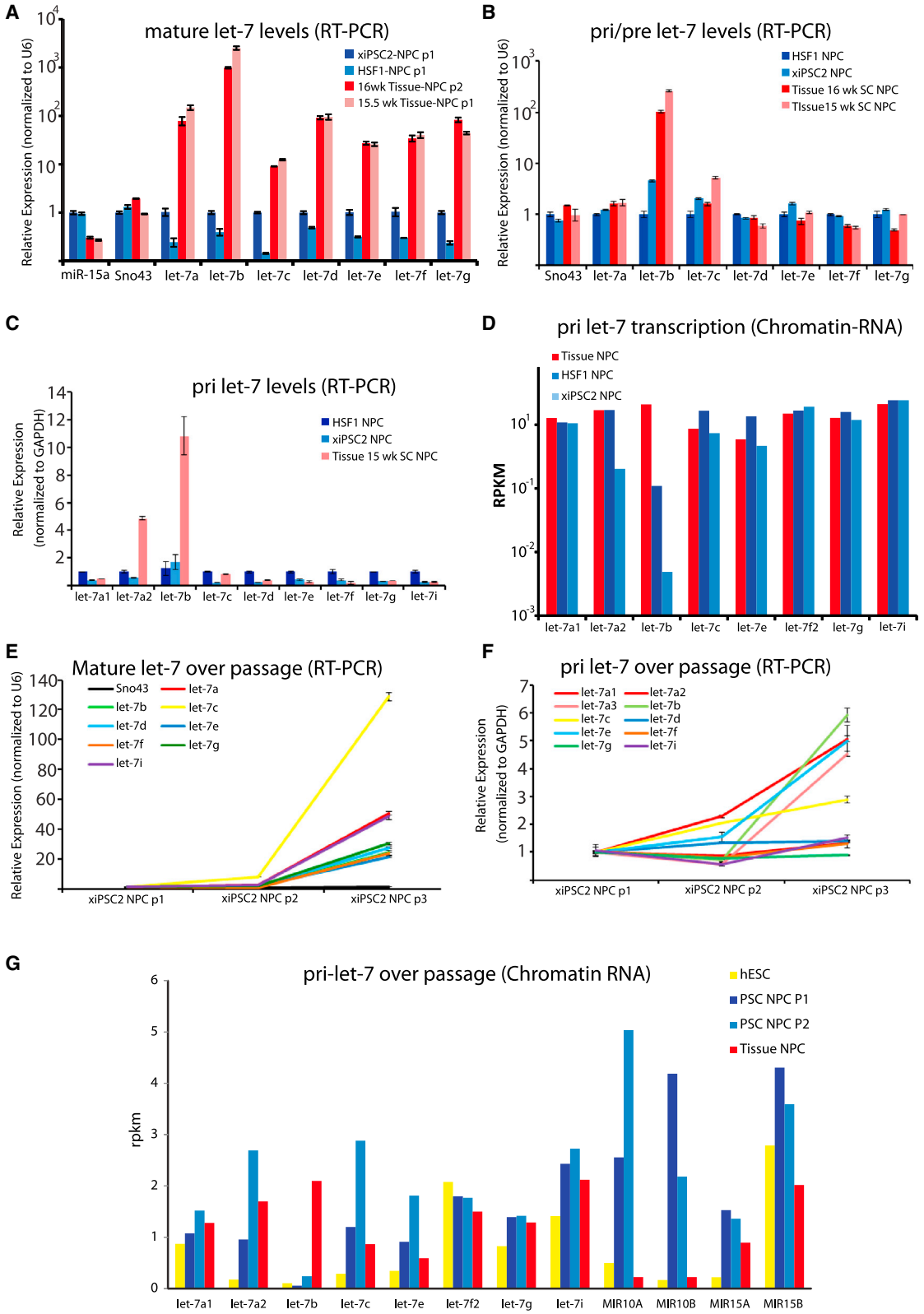

(legend on next page)

opposed to in silico prediction, and showed a large degree of polycistronic expression of groups of *let-7* family members (Table S2).

Manipulation of LIN28A/B Shows a Modest Effect on Developmental Maturity of NPCs

To determine what role *LIN28* had on the developmental maturity of NPCs, we utilized two strategies. First, we used a small interfering RNA (siRNA) approach to knockdown both homologs. When si*LIN28A* and si*LIN28B* were introduced by transfection, mRNA for these genes was suppressed by 70%–75% as measured by RT-PCR (Figure S3A). This was also confirmed by western blot (Figure S3B). As a result of this knockdown, mature *let-7* family miRNAs accumulated, as measured by RT-PCR, relative to transfection of a nontarget (siNT) control (Figure S3C). Also of note, siRNAs against both homologs were necessary to observe an induction of the *let-7* family members, demonstrating their known semiredundant roles in *let-7* maturation (Nam et al., 2011).

Microarray profiling identified many genes differentially expressed as a result of si*LIN28A/B* dual knockdown. However, these differentially expressed genes did not significantly overlap with the original list of probe sets differentially expressed between PSC-NPCs and their tissue-derived counterparts (Figure S3H; Patterson et al., 2012), nor were *let-7* downstream targets, besides *LIN28A* and *LIN28B*, selectively knocked down (Figure S3F). In addition, the dual knockdown had no effect on the propensity to differentiate into neurons or glia (Figure S3D). These findings suggested that RNAi based knockdowns can lower *LIN28* expression and induce *let-7* maturation, but the resulting subtle *let-7* induction exerted little effect functional effect. The second strategy to assess the functional relevance of *LIN28B* in NPC maturation utilized re-expression in Tissue-NPCs. When *LIN28B* was overexpressed in Tissue-NPCs by viral infection, mature *let-7* levels decreased (Figure S3E), a portion of the differentially expressed genes between Tissue-NPCs and PSC-NPCs were corrected (Figure S3H), including some *let-7* target genes (Figure S3F). Importantly, neurogenesis was promoted at the expense of gliogenesis upon induction of *LIN28B* in Tissue-NPCs (Figure S3G).

Direct Manipulation of *let-7* Levels Alters Cell Fate in Neural Progenitors

Previous studies either did not directly address the role of *let-7* in *LIN28*-mediated developmental progression or ruled it out altogether (Balzer et al., 2010; Yuan et al., 2012). To assay whether *let-7* miRNAs play a role in Tissue-NPCs, we introduced antagomirs against *let-7b* and *let-7g*. Microarray analysis on two independent experiments demonstrated that *HMGA2* specifically was strongly induced by antagomirs compared to nonspecific controls at both the RNA and protein levels (Figures 3A and 3B). Looking at global gene expression, 649 probe sets were differentially expressed between *let-7b/g* antagomir-treated and nontarget controls (antag CTRL). Of these probe sets, 181 overlapped with previous comparisons between PSC- and Tissue-NPCs ($p = 3.72 \times 10^{-55}$, Figure 3C), and *let-7* targets were specifically increased in these cells as expected (Figure 3D). Furthermore, Tissue-NPCs transfected with *let-7b/g* antagomirs were significantly more similar to PSC-NPCs than antag-CTRL-transfected cells on a global transcriptome level as measured by Pearson correlation (Figure 3E). Together, these data indicated that levels of *let-7* in PSC- and Tissue-NPCs play a role in the transcriptional disparity between these sources of NPCs, and that manipulation of *let-7* levels can shrink the dissimilarity between them. Finally, when antagomirs against *let-7b/g* were introduced into Tissue-NPCs, they became significantly more neurogenic and less gliogenic (Figure 3F; $p < 0.005$).

Figure 2. Dynamics of *let-7* Expression and Processing between PSC-NPCs and Tissue-NPCs

(A) RT-PCR for mature *let-7* family members normalized against small nucleolar RNA U6 in two PSC-NPCs and two Tissue-NPCs. miR-15a and Sno43 were assayed as controls.

(B) Real-time RT-PCR for pre and pri *let-7* family members normalized against small nucleolar RNA U6.

(C) Real-time RT-PCR for pri-*let-7* miRNAs normalized against the relative levels of GAPDH in each cell type.

(D) miRNA-seq of chromatin-associated primary *let-7* family miRNA transcripts between PSC-NPCs and Tissue-NPCs displayed as reads per kilobase measured (RPKM).

(E) Real-time RT-PCR for mature *let-7* family miRNAs in PSC-NPCs over three passages normalized against U6. Sno43 was run as a negative control and was unchanged over passage.

(F) Real-time RT-PCR for primary *let-7* family miRNA transcripts in PSC-NPCs over three passages normalized against U6.

(G) miRNA-seq of chromatin-associated primary *let-7* family miRNA transcripts in PSC-NPCs over two passages (n = 2 for each group) displayed as reads per kilobase measured (RPKM). Data for miRs-10a, 10b, 15a, and 15b are shown to indicate that *let-7* transcriptional regulation is unique in PSC versus Tissue-NPCs, even over passage, where *let-7a1*, *a2*, *b*, *c*, and *e* were induced. Error bars in all RT-PCR graphs represent SEM over three to four technical replicates, and results shown are representative of at least three independent experiments.

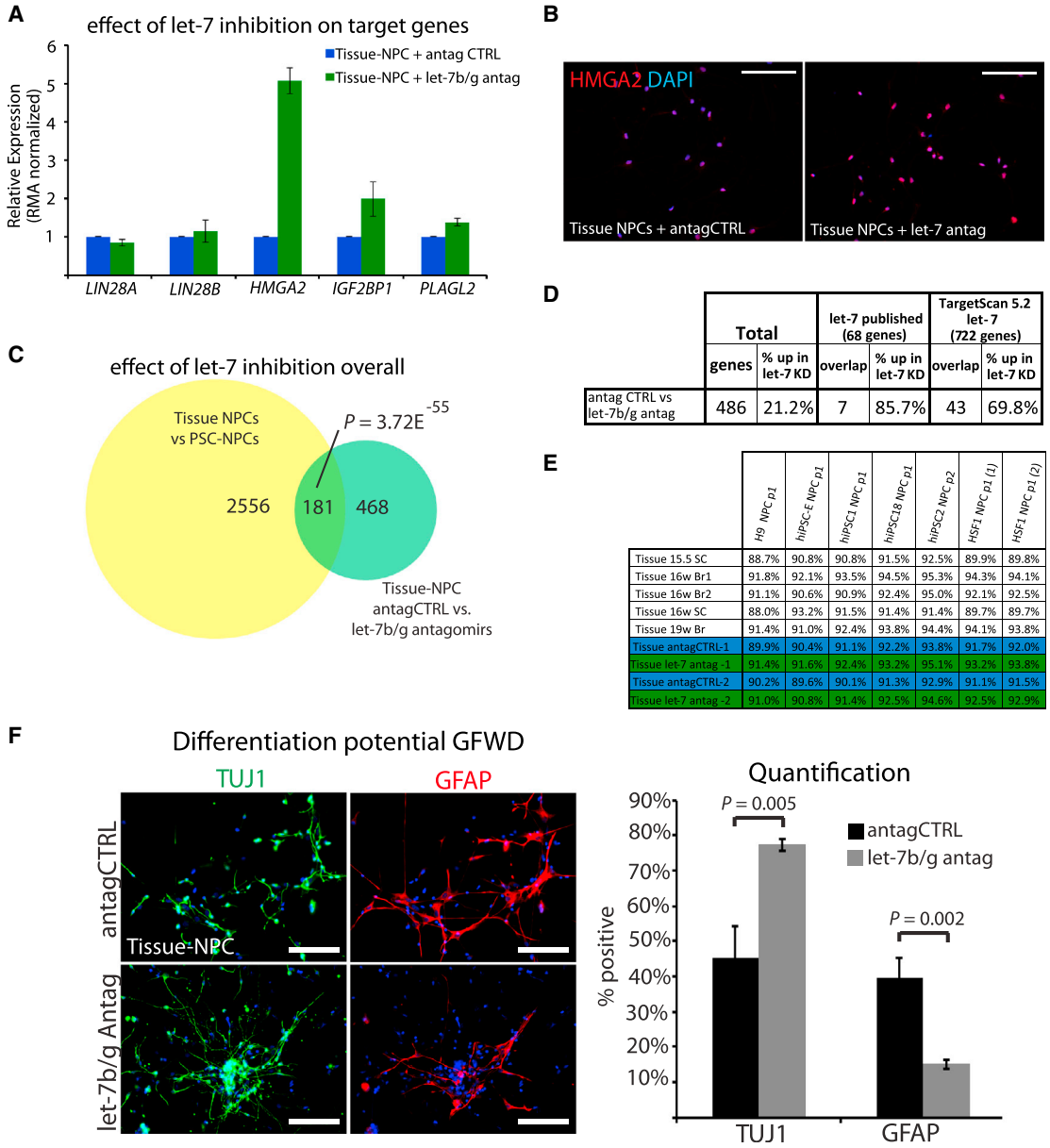

	Total		let-7 published (68 genes)		TargetScan 5.2 let-7 (722 genes)	
	genes	% up in let-7 KD	overlap	% up in let-7 KD	overlap	% up in let-7 KD
antag CTRL vs let-7b/g antag	486	21.2%	7	85.7%	43	69.8%

	H9 NPC p1	hiPSC-E NPC p1	hiPSC1 NPC p1	hiPSC18 NPC p1	hiPSC2 NPC p2	HSF1 NPC p1 (1)	HSF1 NPC p1 (2)
Tissue 15.5 SC	88.7%	90.8%	90.8%	91.5%	92.5%	89.9%	89.8%
Tissue 16w Br1	91.8%	92.1%	93.5%	94.5%	95.3%	94.3%	94.1%
Tissue 16w Br2	91.1%	90.6%	90.9%	92.4%	95.0%	92.1%	92.5%
Tissue 16w SC	88.0%	93.2%	91.5%	91.4%	91.4%	89.7%	89.7%
Tissue 19w Br	91.4%	91.0%	92.4%	93.8%	94.4%	94.1%	93.8%
Tissue antagCTRL-1	89.9%	90.4%	91.1%	92.2%	93.8%	91.7%	92.0%
Tissue let-7 antag -1	91.4%	91.6%	92.4%	93.2%	95.1%	93.2%	93.8%
Tissue antagCTRL-2	90.2%	89.6%	90.1%	91.3%	92.9%	91.1%	91.5%
Tissue let-7 antag -2	91.0%	90.8%	91.4%	92.5%	94.6%	92.5%	92.9%

Figure 3. A Role for LIN28/*let-7* in the Developmental Progression of Human Tissue-NPCs

(A) Averaged robust multiarray average (RMA) normalized expression of selected *let-7* target genes in Tissue-NPCs transfected with *let-7b/g* antagomiRs or nontargeted control antagomiRs by gene expression microarray. Error bars represent SEM across two biological replicates.

(B) Immunostaining for *HMGA2* in Tissue-NPCs showed that *let-7* antagomirs induce *HMGA2* at the protein level.

(C) Venn diagram demonstrating the original differences identified by Patterson et al. (2012) (yellow) and the overlap with gene expression differences (>1.54-fold change) between *let-7b/g* antagomirs versus nonspecific control (antagCTRL) in Tissue-NPCs (green; n = 2).

(D) Overlap of published and predicted *let-7* targets with genes changed after transfection of Tissue-NPCs with *let-7b/g* antagomiRs or nontargeted control antagomiRs measured by gene expression microarray.

(E) Pearson correlations of global gene expression similarity between Tissue-NPCs, Tissue-NPCs transfected with *let-7b/g* antagomiRs or nontargeted control antagomiRs, and PSC-NPCs.

(F) Immunofluorescence (LEFT) and quantification (RIGHT) for TUJ1 (neurons) and GFAP (glia) on Tissue-NPCs differentiated for 3 weeks in growth factor withdrawal following transfection with *let-7b/g* antagomirs or antag CTRL. p value was calculated with Student's t test for at least 1,200 cells across eight to ten fields of view. Error bars represent SEM over fields of view, and results shown are representative of at least three independent experiments. Scale bar, 100 μm.

To determine whether gliogenesis in PSC-NPCs could be regulated by *let-7*, mature oligonucleotides (mimics) for *let-7b* and *let-7g* were transfected into PSC-NPCs. Several *let-7* targets (*LIN28A*, *LIN28B*, *HMGA2*, *IGF2BP1*, and *PLAGL2)* were suppressed as measured by microarray profiling (Figure 4A). Global expression analysis of the of *let-7* mimic-treated NPCs over two independent experiments identified 331 probe sets differentially expressed between *let-7b/g*-transfected PSC-NPCs over respective nonspecific mimic control (miCTRL). Furthermore, among the transcriptional differences observed between these two conditions a significant number overlapped with the original list of genes differentially expressed between PSC- and Tissue-NPCs ($p = 3.76 \times 10^{-46}$, Figure 4B). Focusing on direct *let-7* downstream targets, expression profiling determined that not only were *let-7* target genes overrepresented in the data, but they were specifically downregulated in *let-7b/g*-transfected NPCs over miCTRLs (Figure 4C). Furthermore, *let-7b/g*-transfected PSC-NPCs were significantly more similar to 16–19 week tissue-NPCs than miCTRL-transfected PSC-NPCs on a transcriptome level as measured by Pearson correlation (Figure 4D). Following *let-7* induction, the PSC-NPCs were differentiated for 3 weeks in growth factor withdrawal media. miCTRL-transfected NPCs overwhelmingly produced $TUJ1^+$ neurons, whereas only rare $GFAP^+$ cells were found. When *let-7b/g* mimics were transfected prior to differentiation, the PSC-NPCs were slightly less neurogenic and significantly more gliogenic (Figure 4E; $p = 3.58E^{-05}$).

Taken together, experiments that employed direct regulation of *let-7* levels showed significant effects in both PSC- and Tissue-NPCs at both the molecular and functional levels, whereas attempts to manipulate *LIN28A/B* yielded more subtle effects. This observation is summarized in Figure S3, where manipulation of *LIN28A/B* only showed modest effects on both gene expression and differentiation in NPCs (Figures S3G and S3H). Instead, direct manipulation of *let-7* clearly shows that this miRNA family can control the fate of NPCs (Figures 3 and 4), in contrast to what was shown in a murine model (Balzer et al., 2010).

let-7 Acts through HMGA2 to Control Cell Fate

We hypothesized that the key *let-7* target genes responsible for cell fate in our model should show differences in gene expression levels in experimental settings presented here where NPC fate was affected (Figures 1A, 4E, and 5F). Taking the genes changed in every experimental model we produced that correlated with changes in neurogenesis versus gliogenesis, we narrowed the list of candidate genes. We furthered narrowed the list by taking gene expression data from the Allen Brain Atlas to identify genes changed from the pregliogenic state to the gliogenic stage (8–9 weeks PCW versus 16–18 weeks postconception) (Figure 6A). Just six genes appeared to have expression patterns that correlate with the switch from neurogenesis to gliogenesis in all these settings (Figure 5A). Of these six genes, two were predicted *let-7* target genes (*HMGA2* and *GABBR2*), but only *HMGA2* has been implicated in neurogenesis (Sanosaka et al., 2008). *HMGA2* was shown to affect cell fate in the murine brain (Nishino et al., 2008; Sanosaka et al., 2008) as well as various tissues (Monzen et al., 2008; Yu et al., 2013) and is thought to be mostly expressed prenatally (Ayoubi et al., 1999; Gattas et al., 1999). We found that *HMGA2* was among the genes whose expression was limited to fetal brain prior to 10 weeks of gestation, just prior to the surge of gliogenesis predicted by the Allen Database (Figure 1F).

A closer look at *HMGA2* transcription shows that at least eight transcripts are produced from this locus. One of these transcripts contains a large 3′ UTR that contains six *let-7* binding sites, whereas the other transcripts are predicted to be much less sensitive to suppression by *let-7*. Reanalysis of expression analysis by array with various probe sets that each recognize distinct transcripts showed that the dominant transcript expressed contains multiple *let-7* sites (identified by 208025_s_at), and that this is the only one affected by *let-7* manipulation (data not shown; Figure 5B). Furthermore, this particular transcript is the only one differentially expressed between PSC- and Tissue- NPCs (Figure 5B). The difference in expression of *HMGA2* between Tissue- and PSC- NPCs was also obvious at the protein level (Figure 5C). Taken together, these data suggested that suppression of *HMGA2* levels by induction of *let-7* correlated with the switch from neurogenesis to gliogenesis in the nervous system. To directly test the role of *HMGA2* in the developmental progression of PSC-NPCs, we silenced this gene by RNAi prior to terminal differentiation. Three distinct siRNAs were used (a–c), and just one of them (siHMGA2b) was predicted to target the long isoform with *let-7* sites. *HMGA2* message was suppressed by this method at both the RNA (Figure 5D, left) and protein levels (Figure 5D, right). As with induction of *let-7* mimics, suppression of *HMGA2* significantly induced gliogenesis in PSC-NPCs (Figure 5E).

The Notch Pathway Is a Key Effector of *let-7* in Gliogenesis

Profiling RNA expression after HMGA2 KD uncovered a modest number of genes changed. Intersection of these genes with those that were changed during human neurogenesis (Allen Database) or in Tissue-NPCs where *let-7* was inhibited by antagomirs found just two genes consistently altered (*HES5* and *USP44*)(Figure 6A). Significantly, *HES5* is a key target gene and effector of the NOTCH pathway, and perhaps the best known regulator of gliogenesis in mice (Hojo et al., 2000; Kageyama and Ohtsuka, 1999; Kageyama et al., 2008; Ohtsuka et al., 1999, 2001). RT-PCR

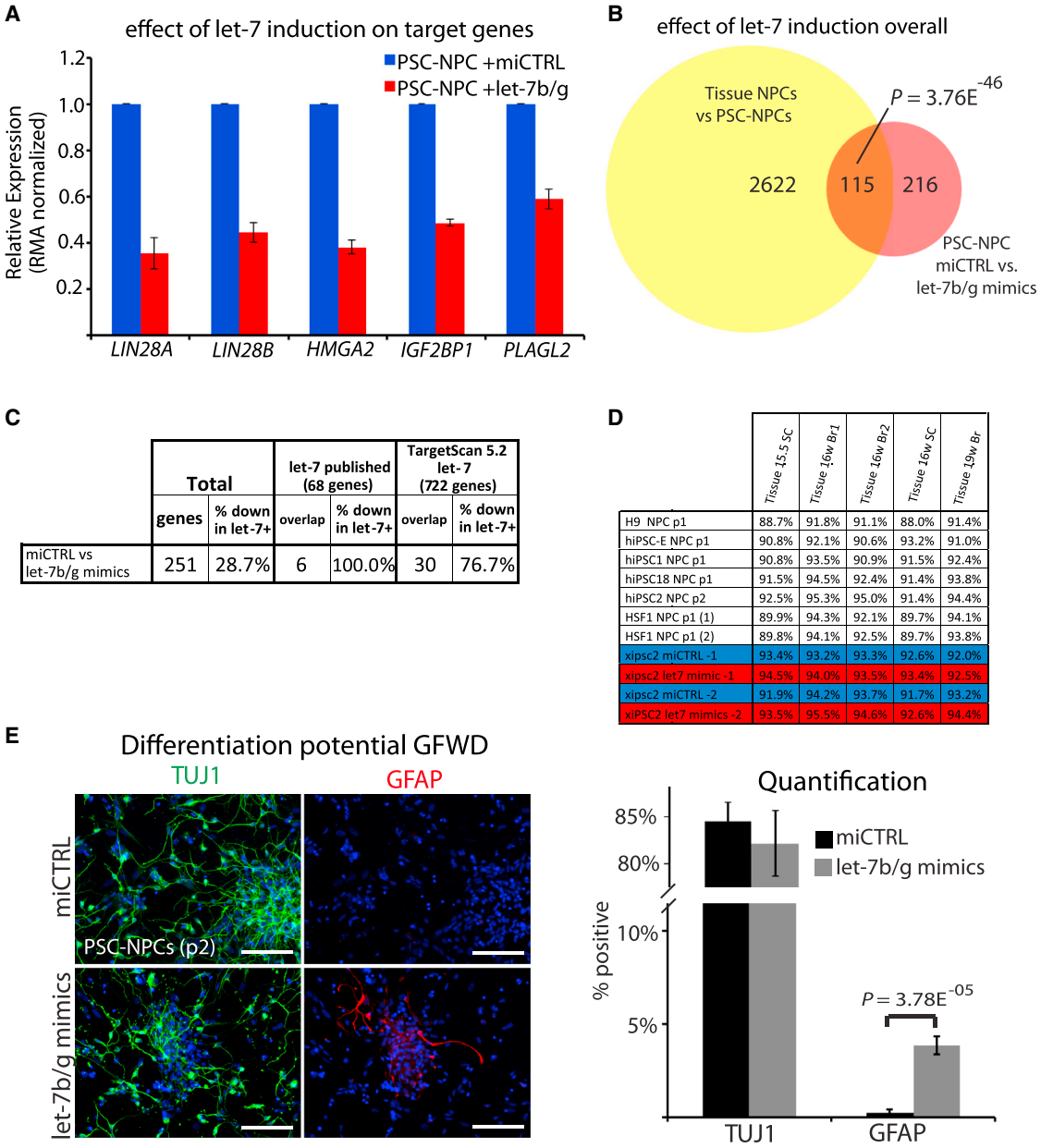

	Total		let-7 published (68 genes)		TargetScan 5.2 let-7 (722 genes)	
	genes	% down in let-7+	overlap	% down in let-7+	overlap	% down in let-7+
miCTRL vs let-7b/g mimics	251	28.7%	6	100.0%	30	76.7%

	Tissue 15.5 SC	Tissue 16w Br1	Tissue 16w Br2	Tissue 16w SC	Tissue 19w Br
H9 NPC p1	88.7%	91.8%	91.1%	88.0%	91.4%
hiPSC-E NPC p1	90.8%	92.1%	90.6%	93.2%	91.0%
hiPSC1 NPC p1	90.8%	93.5%	90.9%	91.5%	92.4%
hiPSC18 NPC p1	91.5%	94.5%	92.4%	91.4%	93.8%
hiPSC2 NPC p2	92.5%	95.3%	95.0%	91.4%	94.4%
HSF1 NPC p1 (1)	89.9%	94.3%	92.1%	89.7%	94.1%
HSF1 NPC p1 (2)	89.8%	94.1%	92.5%	89.7%	93.8%
xipsc2 miCTRL -1	93.4%	93.2%	93.3%	92.6%	92.0%
xipsc2 let7 mimic -1	94.5%	94.0%	93.5%	93.4%	92.5%
xipsc2 miCTRL -2	91.9%	94.2%	93.7%	91.7%	93.2%
xiPSC2 let7 mimics -2	93.5%	95.5%	94.6%	92.6%	94.4%

Figure 4. Direct Introduction of *let-7* miRNAs Affects Developmental Progression of PSC-NPCs

(A) Averaged RMA normalized expression of selected *let-7* target genes in PSC-NPCs transfected with *let-7b/g* mimics or nontargeted control miRNAs by gene expression microarray. Error bars represent SEM across two biological replicates.

(B) Venn diagram demonstrating the original differences identified by Patterson et al. (2012) (yellow), and the overlap with gene expression differences (>1.54-fold change) between *let-7b/g* mimics versus nonspecific control (miCTRL) in PSC-NPCs (red; n = 2).

(C) Overlap of published and predicted *let-7* targets with genes changed after transfection of PSC-NPCs with *let-7b/g* mimics or nontargeted control miRNAs measured by gene expression microarray.

(D) Pearson correlations of global gene expression similarity between PSC-NPCs, PSC-NPCs transfected with *let-7b/g* mimics or nontargeted control miRNAs, and Tissue-NPCs.

(E) Immunofluorescence (left) and quantification (right) for TUJ1 (neurons) and GFAP (glia) on PSC-NPCs differentiated for 3 weeks in growth factor withdrawal following transfection with *let-7b/g* mimics or miCTRL. p value indicated reflects Student's t test for at least 800 cells in multiple wells and across six fields of view. Error bars represent SEM over fields of view, and results shown are representative of at least three independent experiments. Scale bar, 100 μm.

of PSC-NPCs with knockdown of *HMGA2* clearly showed decreased *HES5* levels, suggesting a functional correlation between the two (Figure 6B). This correlation did not appear to be due to a difference in the activity of NOTCH, as both PSC and Tissue-NPCs showed similar activity (Figure 6C). Although NOTCH signaling has been shown to either promote or inhibit gliogenesis depending on the context, in our human model abrogation of all NOTCH signaling with gamma-secretase inhibitor (DAPT) stimulated gliogenesis and suppressed neuronal differentiation (Figure 6D).

Using the Allen database, it is clear that *HES5* is coexpressed with HMGA2 at 8–11 weeks of gestation just prior onset of gliogenesis, and expression of both genes drop significantly thereafter (Figure 6E). On the other hand, most other NOTCH effectors did not significantly change over the same time (Figure S4A). Expression patterns for *HES5* across nine different human cell types representing derivatives of all three germ layers suggested that *HES5* is restricted to the nervous system, whereas the other *HES/HEY* family members had a more widespread distribution throughout various organs (Figures 6F and S4B). This analysis also showed that PSC-NPCs expressed the highest levels of *HES5*, followed by lower expression in Tissue-NPCs, which were more gliogenic (Figure 1A; Patterson et al., 2012).

In order to functionally probe for a link between *HES5* and *let-7*, this miRNA was experimentally abrogated in Tissue-NPCs with antagomirs while suppressing *HES5* induction with siRNA. As shown above (Figure 3F), suppression of *let-7*s with antagomirs increased neurogenesis and decreased gliogenesis in Tissue-NPCs, but when *HES5* induction was simultaneously blocked by siRNA (Figure 6G), this effect was lost (Figure 6H). This result was consistent with the described role for *HES5* in murine neural development in the absence of LIF, whereas, in the presence of LIF, *HES5* has a progliogenic role (Chambers et al., 2001; Chenn, 2009; Hirabayashi and Gotoh, 2005).

As an AT-hook binding protein, *HMGA2* is well known to be broadly associated with chromatin. To begin to understand why *HMGA2* expression strongly correlated with *HES5* levels in NPCs, we probed whether *HMGA2* can regulate access of NICD/RBPj transcriptional complexes to the *HES5* promoter in response to NOTCH activation. Chromatin immunoprecipitation (ChIP) for NICD uncovered significant binding to two RBP binding sites within the *HES5* regulator region (Figure 6I), as expected in cells with strong NOTCH activation (Figure 6C). On the other hand, when *HMGA2* expression was abrogated by siRNA, NICD did not appear to significantly associate with these same sites, consistent with the notion that *HMGA2* plays a role in regulating access of NICD to the *HES5* promoter.

The *let-7* Effect on Gliogenesis Extends to Oligodendrocyte Formation

The fact that induction of *let-7* drove PSC-NPCs toward a more astrocytic fate suggested that *let-7* could play an important role in developmental switches. In the same vein, established protocols to generate oligodendrocytes with PSC-NPCs normally take at least 17 weeks (Stacpoole et al., 2013; Wang et al., 2013), which is akin to the time it takes to produce them in utero (Figure 1F). Using one of these protocols, we observed oligodendrocyte progenitors (OPCs) and mature oligodendrocytes after just 6–7 weeks of culture, but only in PSC-NPCs cultures following *let-7* induction at the NPC stage (Figure 7). These cells were judged to be bona fide oligodendrocytes on the basis of coexpression of O4 and Myelin Basic Protein (MBP) in confocal imaging. This result again suggested that *let-7* can play a role in the developmental maturity of PSC-NPCs and provides an approach to speed the generation of astrocytes and oligodendrocytes from human PSCs.

DISCUSSION

The critical advance of this study is definitively showing that *let-7* levels not only correlate with developmental progression in the human nervous system, but also serve to functionally drive the transition. Furthermore, whereas the *let-7* target gene *HMGA2* had previously been shown to promote neurogenesis in murine NPCs, we showed here that this is also the case for humans as well. Finally, we provide evidence that the mechanism by which *let-7* miRNAs drives progression in the nervous system is by altering expression of a key NOTCH effector gene *HES5*. This NOTCH effector, and NOTCH signaling in general, has been shown to be a promoter of gliogenesis in murine models, whereas our data suggest a proneurogenic role. This discrepancy could be due to several obvious differences in context: murine versus human models, the presence or absence of LIF signaling, and/or in vitro versus in vivo settings. Nevertheless, the effect in this human setting was clear: inhibiting NOTCH activity generated NPCs that went from negligible numbers to a state where over 10% of differentiated cells were astrocytes. We did not try the converse experiment, inducing NOTCH activity, because it appeared as though all NPCs tested, whether neurogenic or gliogenic, showed considerable NOTCH activity. Interestingly, data presented here suggest that no other NOTCH effectors were affected by *let-7* or *HMGA2* manipulation, only *HES5*. These data suggest that the Notch pathway can be regulated by *HES/HEY* effectors by fine-tuning access to the binding sites of its effectors.

However, this study provides only a partial understanding of the relation between HMGA2 and regulation of

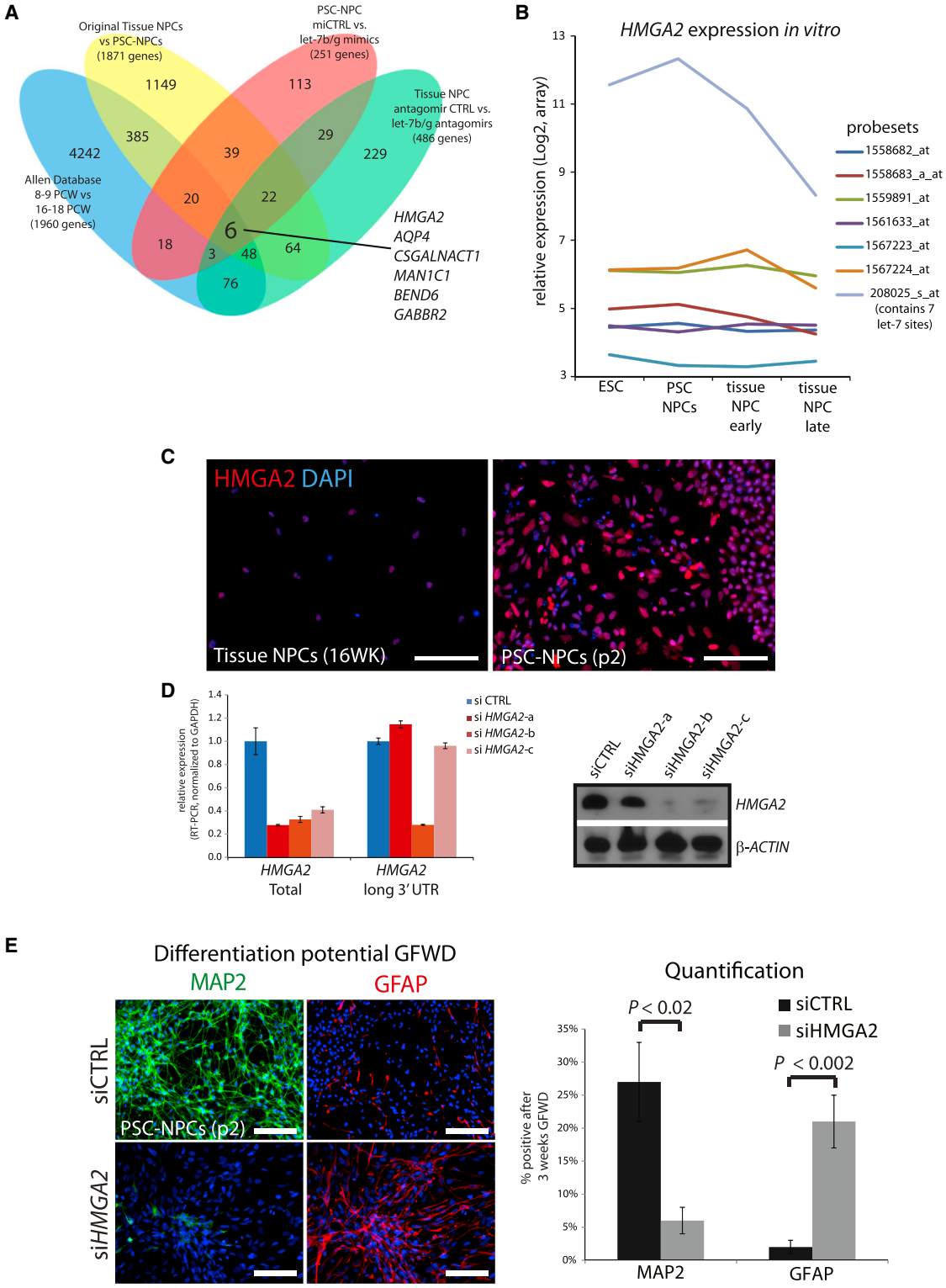

Figure 5. HMGA2 Is a Critical Target of *let-7* in Developmental Progression

(A) Venn diagram demonstrating the overlap of genes changed in comparisons between neurogenic and gliogenic NPCs in the indicated contexts. Original list (yellow): n = 7 PSC-NPC lines and n = 5 Tissue-NPC lines; mimic experiment (red): n = 2 for both mimic- and control-treated lines; antagomir experiment (green): n = 2 for both antag- and control-treated lines.

(legend continued on next page)

Notch signaling. This is due in part to a poorly defined binding pattern of HMGA2 throughout the genome. It is known to be abundant when expressed during development and, as an AT-binding protein, can in theory bind nearly the entire genome. Thus, whereas we show here that the expression of HMGA2 appears to affect access of NICD to the HES5 promoter, it is unclear whether this is due to direct binding at this locus, or a general effect on chromatin compaction.

This study also highlights a role for transcriptional control of let-7 miRNAs in development. It was thought that primary *let-7* transcription occurred at a constant level, and that levels of mature *let-7* were strictly a matter of *LIN28* activity. However, data provided here clearly demonstrate that *let-7b* is regulated at the transcriptional level even in cells that do not express *LIN28A/B*. Our data suggest that, developmentally, one *let-7* family member (pri-*let-7b*) is induced at the transcriptional level prior to the loss of *LIN28A/B* protein and may be a key driver of *LIN28A/B* suppression as gliogenesis is initiated. It will be important to determine whether the methods developed here to facilitate developmental progression also apply to cells that have been transplanted into tissue.

EXPERIMENTAL PROCEDURES

Cell Culture

Undifferentiated hPSC lines HSF1, H9, and xiPSC2 were maintained as previously described (Lowry et al., 2008) and in accordance with UCLA ESCRO. Neural progenitors were derived through formation of neural rosettes and maintained and further differentiated as described (Karumbayaram et al., 2009). NPCs were derived from fetal tissue (either brain or spinal cord) as described. All NPCs were judged to be pure by immunostaining as described (Patterson et al., 2012) (Figure S1).

Transfection

siRNAs (Thermo Dharmacon), *let-7* mimics (Thermo Dharmacon), and *let-7* antagomirs (Thermo Dharmacon "inhibitors") were transfected with Lipofectamine RNAiMAX (Invitrogen) at a ratio of 5 μl lipofectamine:20 nM siRNA or 5 μl lipofectamine:40 nM mimic or antagomirs for each well of a 6-well plate. A reverse transfection method was used. Briefly, Lipofectamine and oligos were premixed in 1 ml of OptiMEM (Gibco) for 25 min in the precoated receiving plate. Cells were then passaged with TrypLE (Gibco), resuspended in 1 ml of NPC media without antibiotics, and plated on top of transfection media. Transfections were incubated overnight at 37°C after which time media was replaced with standard NPC culturing media with antibiotics for the indicated lengths of time. Lentivirus for CMV-LIN28B-SV40-mCherry (Genecopoeia) or UBC-mCherry (Kohn lab) was made by the UCLA vector core. NPCs were reverse infected overnight in NPC media without antibiotic.

Immunostaining

PSC-NPCs or Tissue-NPCs differentiated for 3 weeks were passaged with TrypLE (GIBCO) to glass coverslips 2–7 days before fixing. Coverslips were fixed and stained using standard protocols as described (Patterson et al., 2012). Primary antibodies included rabbit × TUJ1 (1:2,000; Covance), rabbit × GFAP (1:1,000; Dako), rabbit × S100 (1:1,000; Dako), chicken × GFAP (1:2,000, Abcam), mouse × MAP2 (1:500; Abcam), rabbit × Cleaved Notch1 (Val1744) (1:500; Cell Signaling Technologies), rabbit × LIN28A (1:300; Cell Signal), rabbit × LIN28B (1:300; Cell Signal), rabbit × HMGI-C (HMGA2) (1:200, Santa Cruz Biotechnology), mouse × O4 (1:300; R&D Systems), rat × MBP (1:50; Abcam), mouse × A2B5 (1:1,000; Abcam). All images were captured on a Zeiss microscope using Axiovision software (Zeiss) for image capture. GFAP or TUJ1 positive cells were counted using ImageJ software as a percentage of the total DAPI-labeled nuclei or as a percentage of the $mCherry^+$ cells within the field. Average percentage positive cells and SEM was calculated over at least six fields of view. Western blot analysis was performed using standard procedures as described (Lowry et al., 2005). Primary western blot antibodies include rabbit × HMGI-C (1:500; Santa Cruz), rabbit × LIN28A (1:500; Cell Signal), rabbit × LIN28B (1:500; Cell Signal), and mouse × actin (1:1,000).

Additional materials and methods can be found in the Supplemental Information.

SUPPLEMENTAL INFORMATION

Supplemental Information includes Supplemental Experimental Procedures, four figures, and two tables and can be found with this article online at http://dx.doi.org/10.1016/j.stemcr.2014.08.015.

AUTHOR CONTRIBUTIONS

M.P. and X.G.: conception and design, collection and assembly of data, data analysis and interpretation, manuscript writing, final approval of manuscript; K.L., M.E., J.C., Y.X., J.L., S.A., S.M.D.: collection and assembly of data; S.S. and M.P.: data analysis and interpretation; W.E.L.: conception and design, data analysis and

(B) Normalized expression of all probe sets recognizing *HMGA2* in cell types representing developing NPCs. Probe set 208025_s_at is the only one that recognizes the *HMGA2* isoform containing multiple *let-7* target sites.
(C) Immunostaining for *HMGA2* in PSC and Tissue-derived NPCs.
(D) Real-time RT-PCR and western blot for *HMGA2* expression in PSC-NPCs transfected with either control siRNA or each of three different siRNAs against *HMGA2*.
(E) Percentage of positive PSC-NPCs transfected with either control siRNA or siRNA against HMGA2 undergoing neuronal (MAP2) versus glial (GFAP) differentiation following 3 weeks growth factor withdrawal. Images and quantification are representative of three independent experiments. At least 1,900 cells were analyzed across at least eight fields of view. Error bars represent SEM over fields of view, and these data are representative of at least three independent experiments. Scale bar, 100 μm.

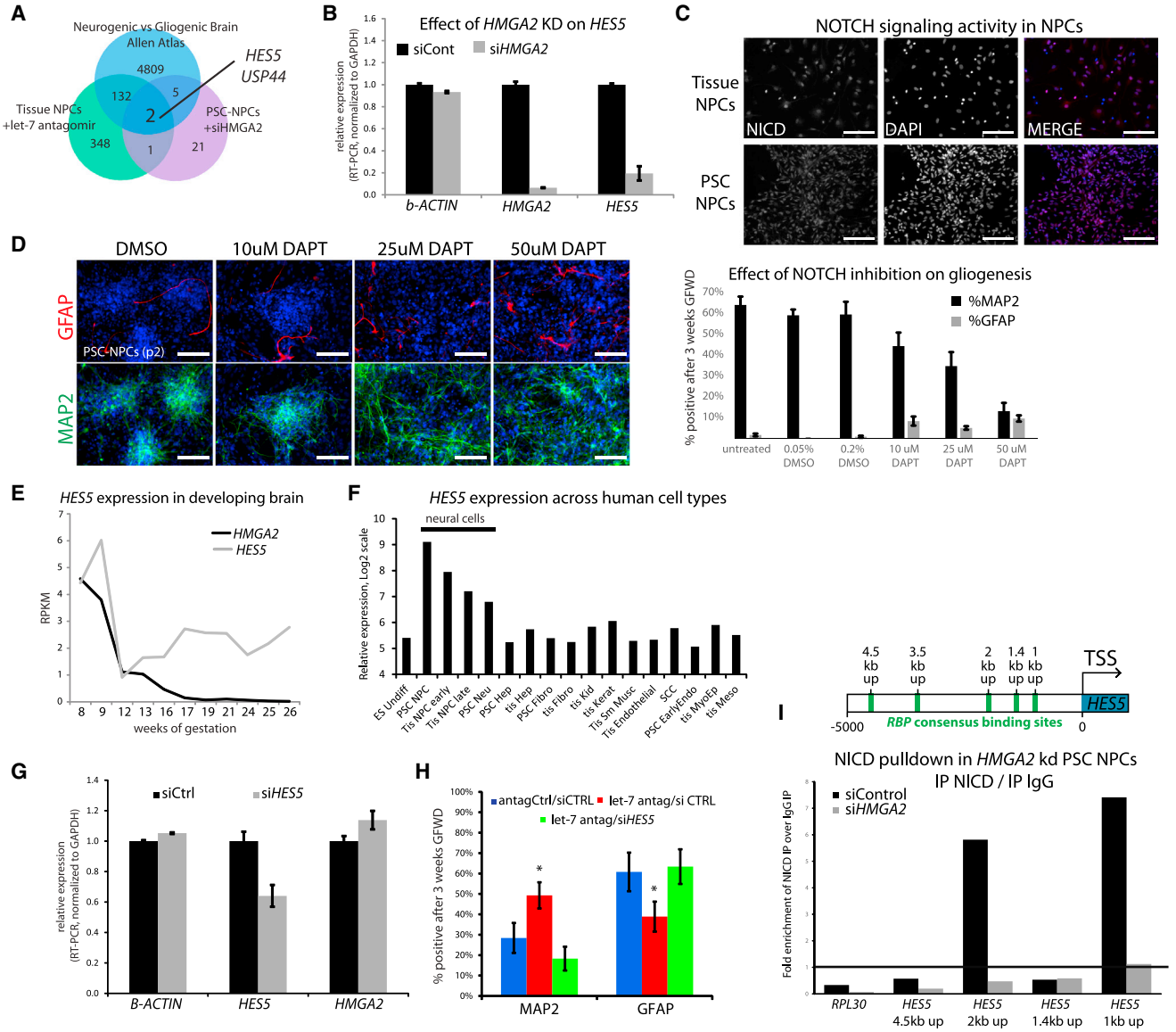

Figure 6. *let-7*/HMGA2 Regulates Notch Sensitivity through HES5

(A) Venn diagram demonstrating overlap of genes changed in comparisons between neurogenic and gliogenic NPCs in the indicated contexts.

(B) RT-PCR for relative expression after siRNA transfection to suppress *HMGA2* expression.

(C) PSC-NPCs and Tissue-NPCs show similar levels of nuclear NICD accumulation suggesting that both have similar activation of the NOTCH pathway. Scale bar, 100 μm.

(D) Using a gamma-secretase inhibitor to block NOTCH activation decreases neuronal differentiation and induces gliogenesis as measured by MAP2 and GFAP staining and quantification. Scale bar, 100 μm.

(E) Transcription of *HMGA2* and *HES5* quantified by RNA-seq across the developing human brain.

(F) Gene expression data taken from an in-house database of a variety of human cell types suggests that *HES5* is mostly expressed in the nervous system, whereas all the other family members are scattered throughout various types of cells from different organs (Log2 scale, RMA transformation).

(G) siRNA silencing of *HES5* shows a 40% knockdown of message compared to scramble control.

(H) As shown previously in Figure 5E, inhibition of *let-7* with antagomirs increased neurogenesis at the expense of gliogenesis. Silencing *HES5* blocks this effect demonstrating a clear link between *let-7* and HES5 activity in neurogenesis. *Student's t test $p < 0.05$ for $n > 450$ cells in multiple wells. Paired t tests were performed for each manipulation, and only those with significant changes were indicated by *. Error bars represent SEM over technical replicates. Results shown are representative of at least three independent experiments.

(legend continued on next page)

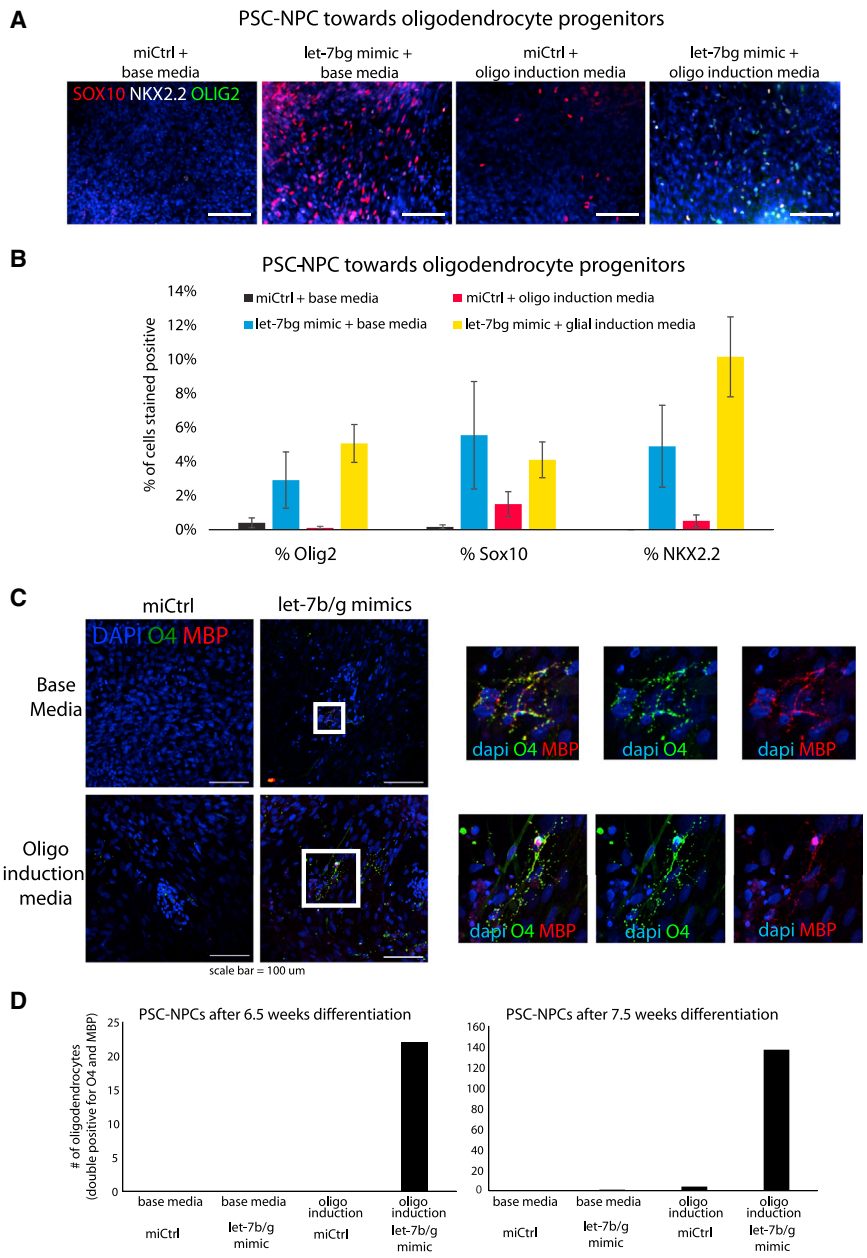

Figure 7. Generation of Oligodendrocytes Is Facilitated by Induction of *let-7*

(A) At 6 weeks of differentiation toward the oligodendrocyte lineage, OPC markers were identified by immunostaining and quantified in (B).

(B) Quantification of results presented in (A).

(C) Following at least 6 weeks of differentiation in either base or glial induction medium, mature oligodendrocytes were identified by immunostaining and quantified in (D). The bottom panels followed a glial induction protocol (Wang et al., 2013) and produced oligodendrocytes after just 6.5 weeks, again, only with *let-7* induction at the NPC stage prior to directed differentiation. At 7.5 weeks, the number of oligodendrocytes produced was considerably larger. Scale bar, 100 mm.

(D) A quantification of oligodendrocytes in each condition at two time points in each well. Cells were judged as bona fide oligodendrocytes if positive for both O4 and MBP.

interpretation, manuscript writing, final approval of manuscript, and financial support.

ACKNOWLEDGMENTS

We would like to thank the core facilities at UCLA (Flow Cytometry Core, EEBRCM; Clinical Genomics, Pathology). We would also like to thank Wen Gu for help with cell-cycle analysis and Gerry Weinmaster for useful suggestions on the Notch pathway. M.P. and Y.X. were supported by a CIRM Training Grant (TG2-01169). X.G. was supported by the MSTP program, David Geffen School of Medicine at UCLA. W.E.L. was supported by the Maria Rowena Ross Chair in Cell Biology and Biochemistry, and this work was supported by grants from CIRM (RB3-05207), NIH (P01GM99134-NIGMS), and

(I) Chromatin immunoprecipitation with antibody against the active NOTCH1 product, NICD, shows strong enrichment for NICD binding in at two predicted RBPj binding sites in the *HES5* upstream region (2 kp up and 1 kb up, see schematic). This enrichment was lost in cells with siHMGA2. Binding is represented as enrichment of pull-down over input and calculated as a function of enrichment of IgG over input. *RPL30* was employed as a negative control locus for a constitutively expressed gene not sensitive to NOTCH1 signaling. Shown is the average of two experiments.

an Eli & Edythe Broad Center of Regenerative Medicine and Stem Cell Research at UCLA Innovation Award.

Received: January 19, 2014
Revised: August 27, 2014
Accepted: August 28, 2014
Published: October 2, 2014

REFERENCES

Ayoubi, T.A., Jansen, E., Meulemans, S.M., and Van de Ven, W.J. (1999). Regulation of HMGIC expression: an architectural transcription factor involved in growth control and development. Oncogene *18*, 5076–5087.

Balzer, E., Heine, C., Jiang, Q., Lee, V.M., and Moss, E.G. (2010). LIN28 alters cell fate succession and acts independently of the let-7 microRNA during neurogliogenesis in vitro. Development *137*, 891–900.

Bhatt, D.M., Pandya-Jones, A., Tong, A.J., Barozzi, I., Lissner, M.M., Natoli, G., Black, D.L., and Smale, S.T. (2012). Transcript dynamics of proinflammatory genes revealed by sequence analysis of subcellular RNA fractions. Cell *150*, 279–290.

Chambers, C.B., Peng, Y., Nguyen, H., Gaiano, N., Fishell, G., and Nye, J.S. (2001). Spatiotemporal selectivity of response to Notch1 signals in mammalian forebrain precursors. Development *128*, 689–702.

Chang, C.J., Mitra, K., Koya, M., Velho, M., Desprat, R., Lenz, J., and Bouhassira, E.E. (2011). Production of embryonic and fetal-like red blood cells from human induced pluripotent stem cells. PLoS ONE *6*, e25761.

Chenn, A. (2009). A top-NOTCH way to make astrocytes. Dev. Cell *16*, 158–159.

Cimadamore, F., Amador-Arjona, A., Chen, C., Huang, C.T., and Terskikh, A.V. (2013). SOX2-LIN28/let-7 pathway regulates proliferation and neurogenesis in neural precursors. Proc. Natl. Acad. Sci. USA *110*, E3017–E3026.

Craig, A., Ling Luo, N., Beardsley, D.J., Wingate-Pearse, N., Walker, D.W., Hohimer, A.R., and Back, S.A. (2003). Quantitative analysis of perinatal rodent oligodendrocyte lineage progression and its correlation with human. Exp. Neurol. *181*, 231–240.

Dean, J.M., Moravec, M.D., Grafe, M., Abend, N., Ren, J., Gong, X., Volpe, J.J., Jensen, F.E., Hohimer, A.R., and Back, S.A. (2011). Strain-specific differences in perinatal rodent oligodendrocyte lineage progression and its correlation with human. Dev. Neurosci. *33*, 251–260.

Gattas, G.J., Quade, B.J., Nowak, R.A., and Morton, C.C. (1999). HMGIC expression in human adult and fetal tissues and in uterine leiomyomata. Genes Chromosomes Cancer *25*, 316–322.

Graf, R., Munschauer, M., Mastrobuoni, G., Mayr, F., Heinemann, U., Kempa, S., Rajewsky, N., and Landthaler, M. (2013). Identification of LIN28B-bound mRNAs reveals features of target recognition and regulation. RNA Biol. *10*, 1146–1159.

Hagan, J.P., Piskounova, E., and Gregory, R.I. (2009). Lin28 recruits the TUTase Zcchc11 to inhibit let-7 maturation in mouse embryonic stem cells. Nat. Struct. Mol. Biol. *16*, 1021–1025.

Heo, I., Joo, C., Cho, J., Ha, M., Han, J., and Kim, V.N. (2008). Lin28 mediates the terminal uridylation of let-7 precursor MicroRNA. Mol. Cell *32*, 276–284.

Hirabayashi, Y., and Gotoh, Y. (2005). Stage-dependent fate determination of neural precursor cells in mouse forebrain. Neurosci. Res. *51*, 331–336.

Hojo, M., Ohtsuka, T., Hashimoto, N., Gradwohl, G., Guillemot, F., and Kageyama, R. (2000). Glial cell fate specification modulated by the bHLH gene Hes5 in mouse retina. Development *127*, 2515–2522.

Jakovcevski, I., Filipovic, R., Mo, Z., Rakic, S., and Zecevic, N. (2009). Oligodendrocyte development and the onset of myelination in the human fetal brain. Front Neuroanat. *3*, 5.

Kageyama, R., and Ohtsuka, T. (1999). The Notch-Hes pathway in mammalian neural development. Cell Res. *9*, 179–188.

Kageyama, R., Ohtsuka, T., and Kobayashi, T. (2008). Roles of Hes genes in neural development. Dev. Growth Differ. *50* (*Suppl 1*), S97–S103.

Karumbayaram, S., Novitch, B.G., Patterson, M., Umbach, J.A., Richter, L., Lindgren, A., Conway, A.E., Clark, A.T., Goldman, S.A., Plath, K., et al. (2009). Directed differentiation of human-induced pluripotent stem cells generates active motor neurons. Stem Cells *27*, 806–811.

Kim, V.N., and Nam, J.W. (2006). Genomics of microRNA. Trends Genet. *22*, 165–173.

Lee, S.H., Cho, S., Sun Kim, M., Choi, K., Cho, J.Y., Gwak, H.S., Kim, Y.J., Yoo, H., Lee, S.H., Park, J.B., and Kim, J.H. (2014). The ubiquitin ligase human TRIM71 regulates let-7 microRNA biogenesis via modulation of Lin28B protein. Biochim. Biophys. Acta *1839*, 374–386.

Lowry, W.E., Blanpain, C., Nowak, J.A., Guasch, G., Lewis, L., and Fuchs, E. (2005). Defining the impact of beta-catenin/Tcf transactivation on epithelial stem cells. Genes Dev. *19*, 1596–1611.

Lowry, W.E., Richter, L., Yachechko, R., Pyle, A.D., Tchieu, J., Sridharan, R., Clark, A.T., and Plath, K. (2008). Generation of human induced pluripotent stem cells from dermal fibroblasts. Proc. Natl. Acad. Sci. USA *105*, 2883–2888.

Mariani, J., Simonini, M.V., Palejev, D., Tomasini, L., Coppola, G., Szekely, A.M., Horvath, T.L., and Vaccarino, F.M. (2012). Modeling human cortical development in vitro using induced pluripotent stem cells. Proc. Natl. Acad. Sci. USA *109*, 12770–12775.

Monzen, K., Ito, Y., Naito, A.T., Kasai, H., Hiroi, Y., Hayashi, D., Shiojima, I., Yamazaki, T., Miyazono, K., Asashima, M., et al. (2008). A crucial role of a high mobility group protein HMGA2 in cardiogenesis. Nat. Cell Biol. *10*, 567–574.

Nam, Y., Chen, C., Gregory, R.I., Chou, J.J., and Sliz, P. (2011). Molecular basis for interaction of let-7 microRNAs with Lin28. Cell *147*, 1080–1091.

Nishino, J., Kim, I., Chada, K., and Morrison, S.J. (2008). Hmga2 promotes neural stem cell self-renewal in young but not old mice by reducing p16Ink4a and p19Arf Expression. Cell *135*, 227–239.

Nishino, J., Kim, S., Zhu, Y., Zhu, H., and Morrison, S.J. (2013). A network of heterochronic genes including Imp1 regulates temporal changes in stem cell properties. eLife *2*, e00924.

Ohtsuka, T., Ishibashi, M., Gradwohl, G., Nakanishi, S., Guillemot, F., and Kageyama, R. (1999). Hes1 and Hes5 as notch effectors in mammalian neuronal differentiation. EMBO J. *18*, 2196–2207.

Ohtsuka, T., Sakamoto, M., Guillemot, F., and Kageyama, R. (2001). Roles of the basic helix-loop-helix genes Hes1 and Hes5 in expansion of neural stem cells of the developing brain. J. Biol. Chem. *276*, 30467–30474.

Patterson, M., Chan, D.N., Ha, I., Case, D., Cui, Y., Van Handel, B., Mikkola, H.K., and Lowry, W.E. (2012). Defining the nature of human pluripotent stem cell progeny. Cell Res. *22*, 178–193.

Piskounova, E., Viswanathan, S.R., Janas, M., LaPierre, R.J., Daley, G.Q., Sliz, P., and Gregory, R.I. (2008). Determinants of microRNA processing inhibition by the developmentally regulated RNA-binding protein Lin28. J. Biol. Chem. *283*, 21310–21314.

Piskounova, E., Polytarchou, C., Thornton, J.E., LaPierre, R.J., Pothoulakis, C., Hagan, J.P., Iliopoulos, D., and Gregory, R.I. (2011). Lin28A and Lin28B inhibit let-7 microRNA biogenesis by distinct mechanisms. Cell *147*, 1066–1079.

Sanosaka, T., Namihira, M., Asano, H., Kohyama, J., Aisaki, K., Igarashi, K., Kanno, J., and Nakashima, K. (2008). Identification of genes that restrict astrocyte differentiation of midgestational neural precursor cells. Neuroscience *155*, 780–788.

Stacpoole, S.R., Spitzer, S., Bilican, B., Compston, A., Karadottir, R., Chandran, S., and Franklin, R.J. (2013). High yields of oligodendrocyte lineage cells from human embryonic stem cells at physiological oxygen tensions for evaluation of translational biology. Stem Cell Reports *1*, 437–450.

Viswanathan, S.R., and Daley, G.Q. (2010). Lin28: a microRNA regulator with a macro role. Cell *140*, 445–449.

Viswanathan, S.R., Daley, G.Q., and Gregory, R.I. (2008). Selective blockade of microRNA processing by Lin28. Science *320*, 97–100.

Wang, D.J., Legesse-Miller, A., Johnson, E.L., and Coller, H.A. (2012). Regulation of the let-7a-3 promoter by NF-κB. PLoS ONE *7*, e31240.

Wang, S., Bates, J., Li, X., Schanz, S., Chandler-Militello, D., Levine, C., Maherali, N., Studer, L., Hochedlinger, K., Windrem, M., and Goldman, S.A. (2013). Human iPSC-derived oligodendrocyte progenitor cells can myelinate and rescue a mouse model of congenital hypomyelination. Cell Stem Cell *12*, 252–264.

West, J.A., Viswanathan, S.R., Yabuuchi, A., Cunniff, K., Takeuchi, A., Park, I.H., Sero, J.E., Zhu, H., Perez-Atayde, A., Frazier, A.L., et al. (2009). A role for Lin28 in primordial germ-cell development and germ-cell malignancy. Nature *460*, 909–913.

Yu, J., et al. (2007). Induced pluripotent stem cell lines derived from human somatic cells. Science *318*, 1917–1920.

Yu, K.R., Park, S.B., Jung, J.W., Seo, M.S., Hong, I.S., Kim, H.S., Seo, Y., Kang, T.W., Lee, J.Y., Kurtz, A., and Kang, K.S. (2013). HMGA2 regulates the in vitro aging and proliferation of human umbilical cord blood-derived stromal cells through the mTOR/p70S6K signaling pathway. Stem Cell Res. *10*, 156–165.

Yuan, J., et al. (2012). Lin28b reprograms adult bone marrow hematopoietic progenitors to mediate fetal-like lymphopoiesis. Science *335*, 1195–1200.

Zambidis, E.T., Peault, B., Park, T.S., Bunz, F., and Civin, C.I. (2005). Hematopoietic differentiation of human embryonic stem cells progresses through sequential hematoendothelial, primitive, and definitive stages resembling human yolk sac development. Blood *106*, 860–870.

Stem Cell Reports, Volume *3*

Supplemental Information

let-7 miRNAs Can Act through Notch to Regulate Human Gliogenesis

M. Patterson, X. Gaeta, K. Loo, M. Edwards, S. Smale, J. Cinkornpumin, Y. Xie, J. Listgarten, S. Azghadi, S.M. Douglass, M. Pellegrini, and W.E. Lowry

Supplemental Figure Legends

Supplemental Table 1. miRNA sequencing on PSC- and Fetal-derived NPCs Reads from miRNA sequencing for sequences (18-25bp in length) with homology to known miRNAs in 16 week Fetal-NPCs (n=2); 6-7 week Fetal-NPCs (n=2) and PSC-NPCs (n=3). Expression of each miRNA represented by the percent of the total RNA. Data sorted by fold change between 16 week Fetal-NPCs and PSC-NPCs.

Supplemental Table 2. mRNA changes in PSC-NPCs after HMGA2 KD In two independent experiments, *HMGA2* was silenced by siRNA-b. 5 days after transfection, the cells were lysed and array analysis was performed. This list of genes represent those that satisfied at student's t-test ($p < 0.02$) and were changed by at least 1.5 fold.

Supplemental Figure 1. Validation of PSC-NPCs and comparison to Tissue-NPCs

(A) Validation of identity of NPCs used in this manuscript. Shown is a quantification of an immunostaining typical of PSC and Tissue-derived NPCs. The vast majority of the cells are positive for at least SOX1, SOX2 and NESTIN, as shown here. (B) RNA-seq data from the Allen Institute's Brainspan developmental transcriptome database showing the relative expression of *let-7* miRNAs displayed as log-scale reads per kilobase measured (log_2 RPKM). miR-98 was not detectable in this dataset at this timescale. (C) Microarray gene expression data from PSC-derived NPCs (n=30 samples) and Tissue-derived NPCs ranging from 6.5 weeks of gestation to 19 weeks of gestation (n=23 samples) were grouped by origin, RMA normalized, and compared using Genespring GX software. Probsesets identified as significantly changed between the two cell types ($p<0.01$ by unmodified t-test after Benjamini-Hochberg FDR correction) and demonstrating >1.54 fold change in either direction were included. A heatmap was generated for the 5479 microarray probesets satisfying these conditions, and these

probesets were ordered by an unbiased hierarchical clustering algorithm. Probesets were curated manually into 6 cluster. Selected gene symbols are listed right of the heatmap for *let-7* miRNA family members (in black) and a subset of predicted *let-7* targets with the most conserved target sites as generated by Targetscan 6.2 (in blue). Table at right shows Gene Ontology terms significantly enriched in each group ($p<0.01$ after Benjamini-Hochberg correction) and filtered for redundancy.

Supplemental Figure 2. Annotation of *let-7* family members within human genome

Shown is a table to annotate all members of the *let-7* family of miRNAs based on their transcription as measured by Chromatin-RNAseq, followed by mapping onto the human genome (Bhatt et al., 2012).

Supplemental Figure 3. Manipulation of *LIN28A/B* in NPCs

(A) Real-time RT-PCR for *LIN28A* and *LIN28B* normalized to *GAPDH* following transfection of si*LIN28B* alone, si*LIN28A* and si*LIN28B* together, or of non-target control (siNT) 2 and 4 days post transfection. Error bars represent SEM over technical replicates. (B) Western blot against LIN28A, LIN28B, and β-ACTIN proteins following transfection of indicated siRNAs. (C) Real-time RT-PCR of mature let-7 family members following transfection of indicated siRNAs. Error bars represent SEM over technical replicates. (D) results from GFWD assay following siRNA for *LIN28A/B*, indicated no significant effect of silencing *LIN28* on neurogenesis or gliogenesis. (E) RT-PCR from experiments where a retrovirus was used to overexpress *LIN28B* (+ IRES Cherry) in Tissue-NPCs. Levels of mature *let-7* family members demonstrated that LIN28B overexpression suppressed all *let-7* miRNAs. Expression normalized to U6. (F) Genes differentially expressed between Tissue-NPCs overexpressing *LIN28B* or Cherry alone and the number of *let-7* targets represented in the data. *Let-7* target lists were generated from published articles and TargetScan 5.2. (G) Immunostaining and quantification to identify the percent

positive Tissue-NPCs infected with either *LIN28B* or Cherry alone undergoing neuronal (TUJ1) vs. glial (GFAP) differentiation following 3 weeks growth factor withdrawal. Note that in these experiments, only Cherry positive cells were quantified for the indicated differentiation marker. P values for student's t-test are indicated for N > 90 Cherry+ cells in multiple wells. Results shown are representative of three independent experiments. (H) Venns comparing gene expression changes in PSC-NPCs after si*LIN28A/B* treatment, Tissue-NPCs after *LIN28B* overexpression, PSC-NPCs after *let-7b/g* mimic treatment, and Tissue-NPCs after *let-7b/g* antagomiR treatment compared against gene expression differences between PSC-NPCs and Tissue-derived NPCs. Direct manipulations of *let-7* miRNAs are more effective than *LIN28* manipulations at changing the expression of those genes as measured by overlaps in the venn diagrams. (I) Quantification of the number of genes changed and overlap in the experiments listed in H.

Supplemental Figure 4. HES family expression across neural development and various human cell types. (A) Data taken from the Allen Brain Atlas suggests that the expression of most HES family members do not change dramatically. (B) Gene expression data taken from an in-house database of a variety of human cell types suggests that *HES5* is mostly expressed in the nervous system, whereas all the other family members are scattered throughout various types of cells from different organs (Log2 scale, RMA transformation).

Supplementary Materials and Methods

Expression Analysis: mRNA

RNA isolation, mRNA reverse transcription, and real-time PCR were performed as described (Lowry et al., 2008). RNA Microarray profiling was performed with Affymetrix Human HG-U133 2.0 Plus arrays as described (Chin et al., 2009; Lowry et al., 2008). Data were normalized with Robust Multichip Algorithm in Genespring separately from previous analyses performed(Patterson et al., 2011). Probe sets that were not expressed at a raw value of > 50 in

at least 10% of samples were eliminated from further analysis. Only those probe sets that made it past the filtering after both normalizations were included in this analysis. Gene expression differences for the *let-7* manipulations (n=2) and for siRNA experiments (n=2) were identified by a fold change of ≥1.54 in pairwise samples, where both biological replicates had a >1.54 fold change compared to their respective control. For *LIN28B* overexpression experiments (n=3), gene expression differences were identified by a paired student t-test ($p<0.05$) and a fold change of >1.54. Gene expression differences for the original list of genes differentially expressed between PSC-NPCs and Tissue-NPCs were determined as previously described(Patterson et al., 2011). Further statistical analysis for hypergeometric distribution and three-way simulation was performed with R, package 2.9.2 as described(Chin et al., 2009). Overlap with *let-7* target genes was performed in Excel using lists generated either from the literature or from TargetScan 5.2. 77 published targets and 751 Target scan targets were originally identified; however some targets were excluded in later analyses because they were not represented in the normalized, filtered data. Pearson correlations were performed in Excel using all normalized, filtered probe sets. All of the microarray data are included in NIHGEO Dataset 51635 and 47796.

Expression analysis: miRNA and mRNA

miRNA was isolated by stratagene RNA isolation kit. Mature and pre/pri miRNA reverse transcription was performed with miScript reverse transcription kit (Qiagen) and real-time PCR was performed using miScript Sybr Green PCR kit and miScript Primer and Precursor Assays (Qiagen). Samples were normalized against small nucleolar RNAs, U6 and Sno43. pri miRNA alone was treated like mRNA and normalized against GAPDH. miRNA seq was performed with Illumina TruSeq Small RNA Sample Prep Kit - Set A (cat. #: RS-200-0012) for constructing the small RNA library; TruSeq PE Cluster Kit v3 - cBot - HS (cat#: PE-401-3001) for template amplification and TruSeq SBS Kit v3 - HS (200-cycles) (cat#: FC-401-3001) for sequencing.

The sequencing reactions were run on HiSeq 2000 as a pair-end 100bp run. Data were normalized as a percent of the total RNA. Individual reads were aligned to known miRNAs with no more than two mismatches. Individual reads for each miRNA were summed together and summed totals were averaged across cohorts: 16wk Tissue-NPC (n=2); 8 wk Tissue-NPC (n=2); PSC-NPC (n=3). Chromatin isolation and RNA sequencing was performed as described previously (Bhatt et al., 2012). The primers used for RT-PCR on mature miRNAs are proprietary but available from Qiagen as a kit for detection.

Primers used for RT-PCR:

Target	**Forward primer**	**Reverse Primer**
Primers for RT-PCR for relative mRNA levels		
HMGA2 total	ACTTCAGCCCAGGGACAAC	TTGAGCTGCTTTAGAGGGAC
HMGA2 long 3' UTR	GGCCAGCTCATAAAATGGAA	TACTGTTCCATTGGCCACAA
LIN28A	CACAGCCCTACCCTGCTC	CTAGCCCCAATGCACCCTAT
LIN28B	CACCAAGCTGGCTTCAATTA	CGCATTCCAAACATCTACCC
GAPDH	CGACCACTTTGTCAAGCTCA	AGGGGTCTACATGGCAACTG
B-ACTIN	GATCATTGCTCCTCCTGAGC	AAAGCCATGCCAATCTCATC
pri-*let-7a1*	GATTCCTTTTCACCATTCACCCTGGATGTT	TTTCTATCAGACCGCCTGGATGCAGACTTT
pri-*let-7a2*	TGTTTAGTGCAAGACCCAAGG	GACTGCATGCTCCCAGGT
pri-*let-7a3*	CCCTTTGGGGTGAGGTAGTAG	CAGATATTACAGCCACTTCAGGAAA
pri-*let-7b*	GCCCCTCGGAAGATAACTATACA	CAAGTTCATGGTCAGAACAGCTT
pri-*let-7c*	TGAAGCAACATTGGAAGCTG	GCCCAAATCAATGATCCAAG
pri-*let-7d*	TGCCAAGTAGAAGACCAGCA	CACCAAAGCAAAGTAGCAAGG
pri-*let-7e*	CCTGGTCCCTGTCTGTCTGT	CAGCCCAGTGGGGCTAAG
pri-*let-7f*	TTGCTTCTTGTCTTATTTCTCTGTG	TCCTCAGGGAAGGCAATAGA
pri-*let-7g*	CCATTACCTGGTTTCCCAGAGA	GTTCCTCCAGCGCTCCGTT
pri-*let-7i*	CGAGGAAGGACGGAGGAG	ACCAGCACTAGCAAGGCAGT

ChIP-PCR

PSC derived NPCs were crosslinked with 1% PFA and chromatin was extracted and purified using a SimpleChIP Enzymatic Chromatin IP kit with magnetic beads (Cell Signaling). IP was performed with normal Rabbit IgG, Rabbit Histone H3, and Rabbit Cleaved Notch1 (Val1744) (D3B8) antibodies (Cell Signaling). DNA was eluted from the beads and used as template for PCR with Real-Time Roche Lightcycler. Signal was quantified first as a function of the

appropriate input sample with the same primers, and then expressed as a function of enrichment over IgG control.

Primers used:

RPL30 exon 3	AAGTCGCTGGAGTCGATCAA	CGATTACCTCAAAGCTGGGC
HES5 4.5kb upstream	GCCGCTGTCTCTGAAATCTG	CCTCTGGGTGGAAACTCTACT
HES5 2kb upstream	CCGCCATCAATGCCCAGA	CTTGATGGATGCAGGAGGG
HES5 1.4kb upstream	CTGCCTAACCAGCCCTGAT	GCTCCTAGAGACAGGTTGGG
HES5 1kb upstream	AAAGCAAGCCCTACAAGTGC	GCCACTGTTTATGCATGCCA

Supplemental Figure 1

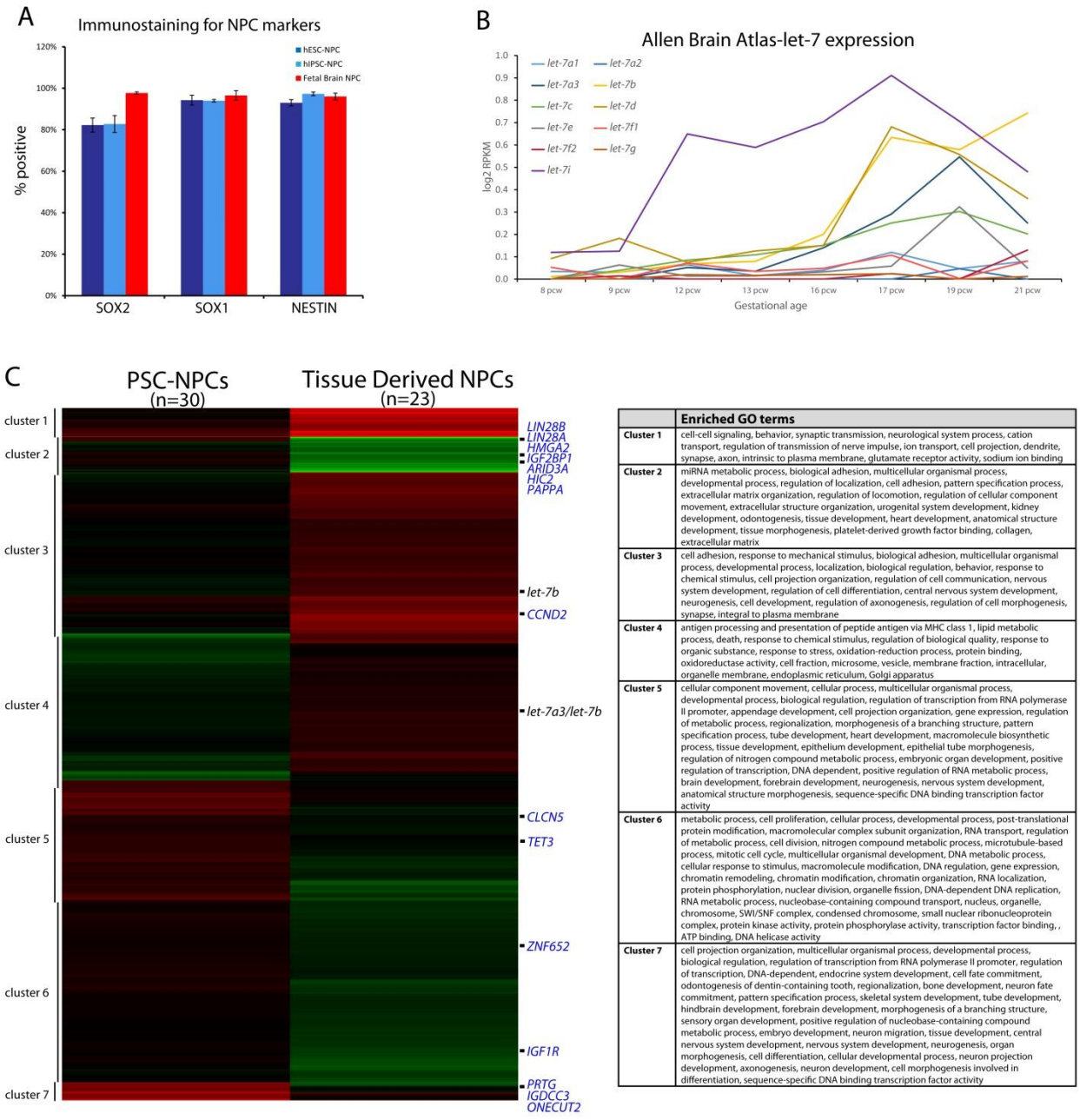

	Enriched GO terms
Cluster 1	cell-cell signaling, behavior, synaptic transmission, neurological system process, cation transport, regulation of transmission of nerve impulse, ion transport, cell projection, dendrite, synapse, axon, intrinsic to plasma membrane, glutamate receptor activity, sodium ion binding
Cluster 2	miRNA metabolic process, biological adhesion, multicellular organismal process, developmental process, regulation of localization, cell adhesion, pattern specification process, extracellular matrix organization, regulation of locomotion, regulation of cellular component movement, extracellular structure organization, urogenital system development, kidney development, odontogenesis, tissue development, heart development, anatomical structure development, tissue morphogenesis, platelet-derived growth factor binding, collagen, extracellular matrix
Cluster 3	cell adhesion, response to mechanical stimulus, biological adhesion, multicellular organismal process, developmental process, localization, biological regulation, behavior, response to chemical stimulus, cell projection organization, regulation of cell communication, nervous system development, regulation of cell differentiation, central nervous system development, neurogenesis, cell development, regulation of axonogenesis, regulation of cell morphogenesis, synapse, integral to plasma membrane
Cluster 4	antigen processing and presentation of peptide antigen via MHC class 1, lipid metabolic process, death, response to chemical stimulus, regulation of biological quality, response to organic substance, response to stress, oxidation-reduction process, protein binding, oxidoreductase activity, cell fraction, microsome, vesicle, membrane fraction, intracellular, organelle membrane, endoplasmic reticulum, Golgi apparatus
Cluster 5	cellular component movement, cellular process, multicellular organismal process, developmental process, biological regulation, regulation of transcription from RNA polymerase II promoter, appendage development, cell projection organization, gene expression, regulation of metabolic process, regionalization, morphogenesis of a branching structure, pattern specification process, tube development, heart development, macromolecule biosynthetic process, tissue development, epithelium development, epithelial tube morphogenesis, regulation of nitrogen compound metabolic process, embryonic organ development, positive regulation of transcription, DNA dependent, positive regulation of RNA metabolic process, brain development, forebrain development, neurogenesis, nervous system development, anatomical structure morphogenesis, sequence-specific DNA binding transcription factor activity
Cluster 6	metabolic process, cell proliferation, cellular process, developmental process, post-translational protein modification, macromolecular complex subunit organization, RNA transport, regulation of metabolic process, cell division, nitrogen compound metabolic process, microtubule-based process, mitotic cell cycle, multicellular organismal development, DNA metabolic process, cellular response to stimulus, macromolecule modification, DNA regulation, gene expression, chromatin remodeling, chromatin modification, chromatin organization, RNA localization, protein phosphorylation, nuclear division, organelle fission, DNA-dependent DNA replication, RNA metabolic process, nucleobase-containing compound transport, nucleus, organelle, chromosome, SWI/SNF complex, condensed chromosome, small nuclear ribonucleoprotein complex, protein kinase activity, protein phosphorylase activity, transcription factor binding, , ATP binding, DNA helicase activity
Cluster 7	cell projection organization, multicellular organismal process, developmental process, biological regulation, regulation of transcription from RNA polymerase II promoter, regulation of transcription, DNA-dependent, endocrine system development, cell fate commitment, odontogenesis of dentin-containing tooth, regionalization, bone development, neuron fate commitment, pattern specification process, skeletal system development, tube development, hindbrain development, forebrain development, morphogenesis of a branching structure, sensory organ development, positive regulation of nucleobase-containing compound metabolic process, embryo development, neuron migration, tissue development, central nervous system development, nervous system development, neurogenesis, organ morphogenesis, cell differentiation, cellular developmental process, neuron projection development, axonogenesis, neuron development, cell morphogenesis involved in differentiation, sequence-specific DNA binding transcription factor activity

Supplemental Figure 2

Let7 family member	Other miRs	Chr	Strand	Start	End	Length (bp)	miRStart Annotation
let7b	4763, 3619	22	+	46,467,707	46,514,431	46,724	Based on one existing MIRLET7B host gene. One of the predicted start sites corellates with chromatin data **TSS 46467598: 109bp difference** **http://mirstart.mbc.nctu.edu.tw/mirna.php?no=50548**
let7a3		22	+	46,467,707	46,514,431	46,724	
let7a2	100, 125B1	11	-	121,961,330	122,076,912	115,582	Longest start site prediction is ~40kb upstream of mature miRNA **http://mirstart.mbc.nctu.edu.tw/mirna.php?no=50546**
let7a1		9	+	96,929,333	96,967,519	38,186	One of the predicted start sites overlaps well with chromatin data and has a block of conservation **TSS: 96929288 45bp difference**
let-7d		9	+	96,929,333	96,967,519	38,186	**http://mirstart.mbc.nctu.edu.tw/mirna.php?no=50545**
let-7f1		9	+	96,929,333	96,967,519	38,186	
let-7c	99A, 125B2	21	+	17,442,842	18,024,259	581,417	**http://mirstart.mbc.nctu.edu.tw/mirna.php?no=50549**
let-7e	99B, 125A	19	+	52,193,049	52,214,933	21,884	One of the predicted start sites overlaps well with chromatin data and has a block of conservation **TSS: 52193273 224bp difference** **http://mirstart.mbc.nctu.edu.tw/mirna.php?no=50551**
let-7f2	98	X	-	53,559,057	53,713,697	154,640	**http://mirstart.mbc.nctu.edu.tw/mirna.php?no=50553**
let-7g		3	-	52,288,438	52,312,659	24,221	**http://mirstart.mbc.nctu.edu.tw/mirna.php?no=50896**
let-7i		12	+	62,993,322	63,024,823	31,501	No predicted site with 3kb start site predicted by Chromatin data. All the other predicted start sites are upstream within another coding gene MON2 **http://mirstart.mbc.nctu.edu.tw/mirna.php?no=50897**

Supplemental Figure 3

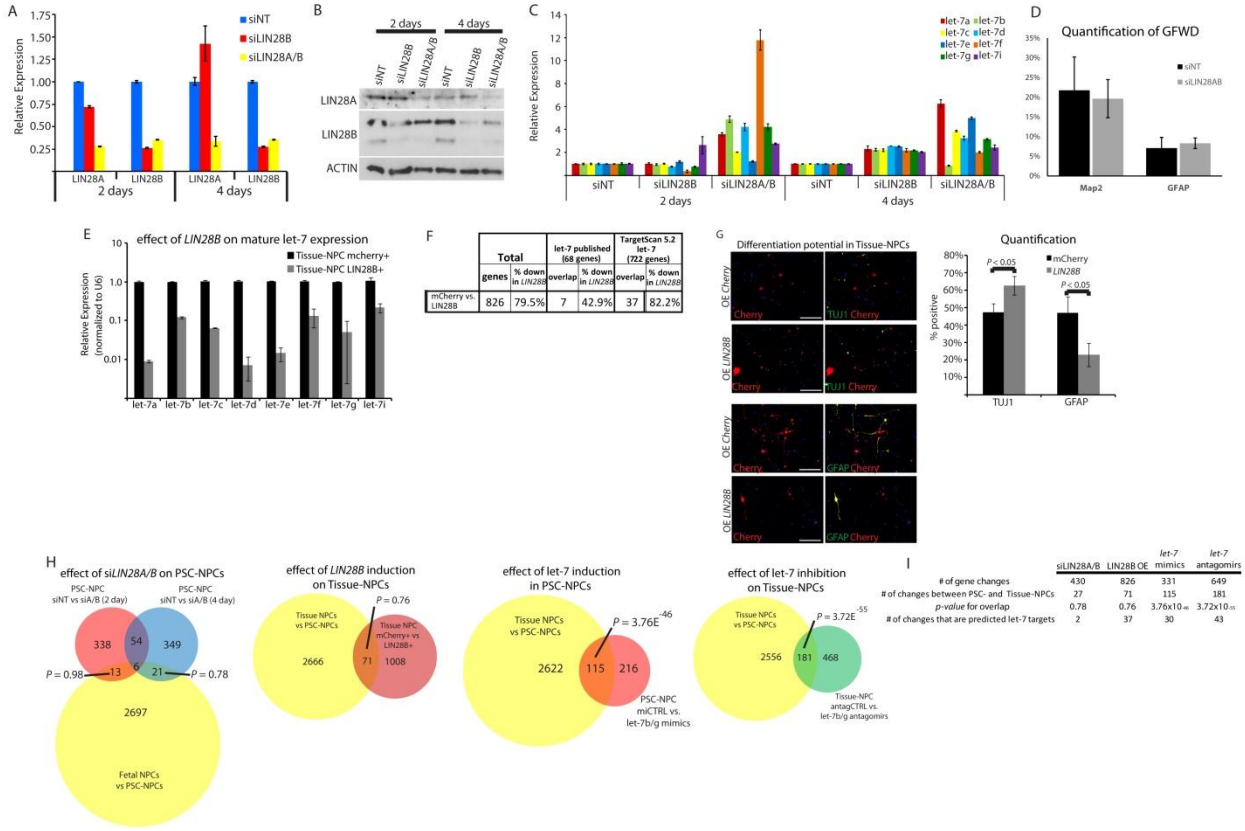

Supplemental Figure 4

A

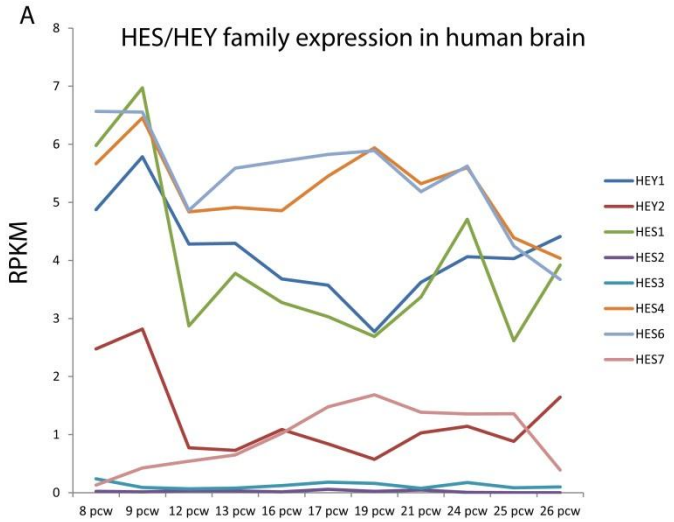

B

Gene of Interest	ES Undiff	PSC NPC	Tis NPC early	Tis NPC late	PSC Neu	PSC Hep	tis Hep	PSC Fibro	tis Fibro	tis Kid	tis Kerat	Tis Sm Musc	Tis Endothelial	SCC	PSC EarlyEndo	tis MyoEp	tis Meso
HMGA2	11.56	12.33	10.87	8.32	10.33	10.78	6.06	11.18	9.13	10.63	11.89	10.37	9.88	11.12	11.42	10.63	9.27
Hes1	8.33	10.68	10.42	9.88	10.84	9.90	8.04	9.57	6.22	7.23	9.77	7.31	9.70	8.04	8.73	7.99	7.64
Hes2	6.71	6.84	6.79	6.59	6.90	6.95	7.88	6.75	6.70	6.72	9.92	6.66	8.51	7.27	6.91	7.81	6.81
Hes4	6.44	10.14	9.10	8.96	9.86	9.49	6.93	8.01	6.25	7.86	8.00	5.91	8.29	8.21	7.21	5.78	6.11
Hes5	5.41	9.11	7.95	7.20	6.79	5.24	5.74	5.39	5.24	5.84	6.06	5.29	5.33	5.78	5.07	5.90	5.52
Hey1	7.49	10.12	10.08	10.68	10.10	9.78	6.43	7.30	6.52	6.64	7.11	6.96	10.24	8.14	8.70	5.77	6.58
Hey2	8.71	7.26	10.26	9.09	9.04	7.65	6.28	5.06	4.80	4.92	4.59	5.78	8.03	5.32	8.69	4.41	4.79
Notch1	8.51	9.78	10.97	10.44	9.95	8.35	8.04	8.13	7.59	8.34	9.97	8.09	10.19	7.77	8.65	8.95	8.13

Supplemental Table 2

Expression in PSC HMGA2 kd v. control PSC NPCs

Gene Name	Fold Change
HES5	4.83
ARHGEF4	2.00
MBTD1	1.98
GAD1	1.97
LUC7L3	1.86
BEND5	1.79
REM2	1.77
SFRP1	1.73
USP44	1.71
DAAM1	1.70
WNT4	1.67
C21orf71	1.61
GABBR2	1.61
DSC3	1.61
LOC147670	1.60
PREX1	1.60
SOX2	1.58
HOXD3	1.57
IKZF4	1.54
FERMT2	-1.57
OXTR	-1.58
ATP11B	-1.62
EYA4	-1.62
TBC1D8B	-1.67
TGFB2	-1.67
CXCL12	-1.68
LIMA1	-1.69
CALD1	-1.70
CCPG1	-1.76
MAN2A1	-1.82
FAR2	-1.87
C12orf39	-1.95
IL1RAP	-2.01
ENPP1	-2.18